Nano Research

ISSN 1998-0124 CN 11-5974/O4
https://doi.org/10.26599/NR.2026.94909283

Research Article

Solution-processable conjugated polymer films via fluorination-induced noncovalent conformational locks for efficient photocatalytic U(VI) removal

Zuojia Li[1,2], Jinwei Shi[1,2], Hanting Wu[2], Yuanping Jiang[1,2](✉), Zhibin Zhang[1,2](✉), Yunhai Liu[2,3]

[1] Jiangxi Province Key Laboratory of Nuclear Physics and Technology, East China University of Technology, Nanchang 330013, China

[2] School of Chemistry and Materials Science, East China University of Technology, Nanchang 330013, China

[3] Gandong University, Fuzhou 344000, China

Nano Res., **Just Accepted Manuscript** • https://doi.org/10.26599/NR.2026.94909283

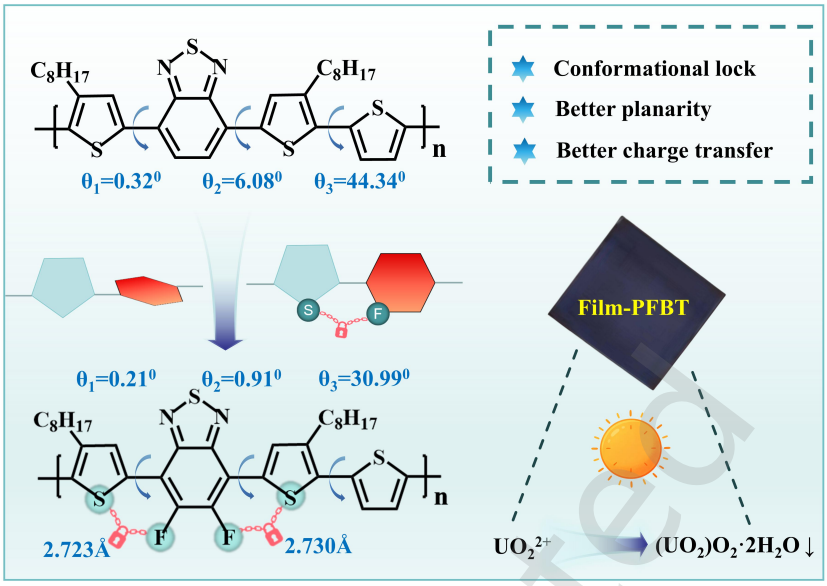
https://www.sciopen.com/journal/1998-0124 on Oct. 25, 2026

© The Authors(s)

Just Accepted

This is a "Just Accepted" manuscript, which has been examined by the peer-review process and has been accepted for publication. A "Just Accepted" manuscript is published online shortly after its acceptance,which is prior to technical editing and formatting and author proofing. Tsinghua University Press (TUP) provides "Just Accepted" as an optional and free service which allows authors to make their results available to the research community as soon as possible after acceptance. After a manuscript has been technically edited and formatted, and the page proofs have been corrected, it will be removed from the "Just Accepted" web site and published officially with volume and article number (e.g., *Nano Research*, **2025**, *18*, 94906990). Please note that technical editing may introduce minor changes to the manuscript text and/or graphics which may affect the content, and all legal disclaimers that apply to the journal pertain. In no event shall TUP be held responsible for errors or consequences arising from the use of any information contained in these "Just Accepted" manuscripts. To cite this anuscript please use its Digital Object Identifier (DOI®),which is identical for all formats of publication.

Just Accepted



This figure illustrates the structure-activity relationship of fluorinated PFBT conjugated polymer photocatalysts: the formation of conformational locks through F···S non-covalent interactions reduces molecular torsional angles, enhances planarity and charge transfer efficiency; under light irradiation, the film material converts UO_2^{2+} into solid-phase $(UO_2)O_2 \cdot 2H_2O$, enabling efficient uranium removal.

Just Accepted

Nano Research

Open Access

Review Article/Research Article Please choose on

Solution-processable conjugated polymer films via fluorination-induced noncovalent conformational locks for efficient photocatalytic U(VI) removal

Zuojia Li[1,2], Jinwei Shi[1,2], Hanting Wu[2], Yuanping Jiang[1,2] ✉, Zhibin Zhang[1,2] ✉, Yunhai Liu[2,3]

[1]*Jiangxi Province Key Laboratory of Nuclear Physics and Technology, East China University of Technology, Nanchang 330013, China*
[2]*School of Chemistry and Materials Science, East China University of Technology, Nanchang 330013, China*
[3]*Gandong University, Fuzhou 344000, China*

Received: 13 August 2026; **Revised:** 19 October 2026; **Accepted:** 25 October 2026

✉Address correspondence to Zhibin Zhang, zhbzhang@ecut.edu.cn; Yuanping Jiang, jypjiang@ecut.edu.cn

Cite this article: *Nano Research*, 2026, 19, 94909283 https://doi.org/10.26599/NR.2026.94909283

ABSTRACT: The practical application of donor-acceptor(D-A) conjugated polymers for photocatalytic U(VI) extraction is limited, fused-ring planar backbones that enable efficient charge transport yet resist film processing and soluble backbones that allow film fabrication yet suffer from poor planarity and photocatalytic activity. Here, we demonstrate that a single fluorination method locked the backbone into a near-planar conformation via F···S simple noncovalent interactions, while simultaneously conferring enough solubility for direct casting of recyclable polymer films. The optimized Film-PFBT, tested in a lab-scale continuous-flow photoreactor, achieves 95% U(VI) removal within 4 hours with a rate constant 1.74 times that of its non-fluorinated control, and retains >60% efficiency even in genuine uranium mining wastewater. This work offers a conjugated polymer photocatalyst design featuring enhanced processability and reusability for potential application in uranium-contaminated water remediation.

KEYWORDS: fluorination; noncovalent conformational lock; conjugated polymer; uranium(VI); photocatalysis

Just Accepted

1.Introduction

Nuclear energy, as a significant low-carbon energy source, plays a critical role in addressing the global energy crisis and achieving carbon neutrality goals[1-3]. Uranium constitutes a critical strategic resource throughout the nuclear fuel cycle. Nevertheless, substantial amounts of radioactive wastewater containing soluble U(VI) are generated during uranium mining, fuel fabrication, and the treatment of nuclear waste liquids, which represent a severe hazard to both the ecosystem and public health[4]. Consequently, the efficient sequestration and recovery of U(VI) from water bodies represent not only a pressing need for radioactive pollution control, but also hold substantial importance for the sustainable advancement of nuclear energy[5, 6].

To date, various strategies have been developed for the removal of U(VI) from aqueous solutions, including adsorption, chemical precipitation, membrane separation, ion exchange, electrochemical reduction, and bioremediation[7]. Among them, adsorption has been the most widely investigated owing to its Photocatalysis offers a mild-conditions route for converting soluble uranyl ions in aqueous media into sparingly soluble uranium-bearing solid phases, and is distinguished by its green chemistry attributes, low energy footprint, and superior treatment efficacy, thus representing a highly promising strategy for the remediation of uranium-contaminated waters[11-13]. simplicity and low cost; however, it generally suffers from limited selectivity, moderate uptake capacity, and the generation of secondary solid waste that requires further treatment. Chemical precipitation and ion exchange are effective at relatively high uranium concentrations, but they are less applicable to trace-level U(VI) and produce large volumes of secondary sludge[8]. Membrane separation offers high selectivity, yet it is constrained by membrane fouling, high energy input, and limited flux. Electrochemical reduction can efficiently immobilize U(VI) but relies on an external power supply and sophisticated electrode engineering[9]. By contrast, photocatalysis converts soluble U(VI) into sparingly soluble U(VI)-bearing solid precipitates under mild conditions driven by renewable solar energy, simultaneously achieving uranium immobilization, waste volume reduction, and enhanced safety of the final waste form[10]. These unique advantages make photocatalysis a highly promising strategy for the remediation of uranium-contaminated waters.

Nevertheless, conventional inorganic photocatalysts are plagued by persistent limitations-namely, narrow visible-light responsiveness, suboptimal charge-carrier separation, and the intractability of band-structure engineering-which collectively impede their practical deployment. By contrast, donor-acceptor (D-A) type conjugated polymers, endowed with adjustable band

structures, broad spectral absorption, and enhanced charge dissociation, have emerged as highly attractive candidates in photocatalytic applications[14, 15]. Among these, the benzothiadiazole (BT) moiety, characterized by its strong electron-withdrawing capability and rigid conjugated planar structure, has been extensively utilized as a high-performance acceptor in the construction of D-A photocatalysts. While existing research has demonstrated the remarkable efficacy of BT-based polymers in the photocatalytic removal of U(VI), their real-world deployment continues to be confronted with challenges on two fronts[15, 16]. First, there are inherent defects at the molecular conformation level. In D-A copolymers, the single bonds connecting the donor units and the BT units are prone to free rotation, resulting in large dihedral angles. This forces the conjugated backbone to deviate from a planar conformation, disrupts the continuity of π-electron delocalization, and suppresses both the intramolecular charge transfer (ICT) efficiency and the migration rate of photogenerated charge carriers, thereby weakening the intrinsic photocatalytic activity of the material[17-19]. Second, there are general limitations associated with powder morphology. Like most powdered photocatalysts, conventionally synthesized BT-based polymers exist in powder form, which exhibits poor dispersibility in aqueous media, a tendency to agglomerate, and difficulty in efficient recovery after reaction. This leads to low recycling efficiency and the risk of secondary pollution. Therefore, addressing the molecular conformational defects and powder morphology issues is fundamental to the application of BT-based photocatalytic materials.

Fluorination modification has been proven to be an effective approach for modulating molecular energy-level structures and planar conformations[20-22]. The strong electronegativity of fluorine atoms can induce changes in molecular dipole moments, optimize frontier orbital energy levels, and promote charge separation. More importantly, fluorine atoms can form non-covalent interactions with heteroatoms on adjacent units, generating a "conformational lock" effect that significantly reduces the dihedral angle between the donor and acceptor, locks the backbone into a near-planar conformation, thereby extending the π-conjugation length and enhancing charge mobility. For example, Gamez-Valenzuela et al[20] confirmed that fluorine atoms form F···S non-covalent interactions with the sulfur atoms of adjacent thiophene rings, sharply reducing the dihedral angle between the isoindigo unit and the thiophene ring from 22° to 4°. This locks the near-planar conformation, extends the π-conjugation length, and improves the efficiency of charge separation; Ahn et al[23] by introducing fluorine atoms into the polymer backbone to form F···S non-covalent "conformational locks" with adjacent sulfur atoms, the planarity of the polymer backbone is significantly enhanced. Benefiting from the efficient charge transport channels provided by this rigid planar structure, the fluorinated polymer BDD-BT achieved excellent high charge carrier mobilities in TGBC-OFET devices, with hole and electron mobilities reaching 0.513 $cm^2 V^{-1} s^{-1}$ and 0.577 $cm^2 V^{-1} s^{-1}$, respectively.

Meanwhile, fabricating the polymer into thin-film materials can not only preserve the rapid charge transport channels arising from molecular-scale ordered packing, but also enable convenient separation and repeated use of the photocatalyst, thereby overcoming the limitations of the powder state[24, 25]. Conventional polymer photocatalysts have generally been optimized for denser π-π stacking and enhanced carrier mobility, often at the expense of solubility, rendering them challenging to process into readily recoverable morphologies such as thin-film architectures[26, 27]. Introducing long-chain alkyl groups into conjugated polymer molecules is an effective method to improve polymer solubility, and this approach has been widely applied in fields such as organic solar cells[28, 29]. Therefore, it becomes possible to enhance the solubility of polymers while ensuring charge carrier mobility by introducing alkyl chains of appropriate length into the polymer molecules.

Based on the above analysis, this paper proposes a synergistic strategy integrating "fluorination-induced conformational locking" and "thin-film engineering". We synthesized two long-chain alkyl-containing polymers, the fluorine-free control PBT and the fluorinated PFBT, via Stille coupling polymerization. Taking advantage of the solubility of both polymers in highly polar organic solvents, we fabricated uniform thin films, designated as Film-PBT and Film-PFBT. The effects of fluorination on molecular dihedral angles, backbone planarity, ICT effects, light absorption, and band structures were systematically investigated, and the performance, stability, and active species mechanisms of the thin-film photocatalysts for U(VI) removal were evaluated. The results showed that Film-PFBT achieved a 95% U(VI) removal rate within 4 hours under visible light. Its excellent performance can be attributed to the enhanced charge separation and transport efficiency resulting from the fluorination-induced conformational lock that reduces the dihedral angle. This study provides a new molecular design strategy for developing efficient, stable, and easily recoverable D-A polymer photocatalysts, and offers valuable reference for advancing the practical application of photocatalytic technology in uranium-containing wastewater treatment.

2.Experimental section

The synthetic procedures for PBT and PFBT are described as follows. Details are provided in the Fig. 1.

(1) Synthesis method of 2, 5-bis (tri-n-butylstannyl) thiophene (Compound 1)[30].

Under a N_2 atmosphere, 2, 5-dibromothiophene (1.21 g, 5 mmol) was dissolved in 20 mL of super-dry THF in a 100 mL two-necked flask and then cooled to -78 °C. Under vigorous stirring, a 2.5 mol/L solution of n-BuLi in hexane (4 mL, 10 mmol) was added dropwise. After the addition was complete, the mixture was stirred for 30 min, followed by the dropwise addition of tri-n-butyltin chloride (3.25 g, 10 mmol). After the addition was complete, the mixture was stirred for 3 h, then allowed to warm to room temperature and stirred for an additional 12 h. After the reaction, an appropriate amount of deionized water was added to quench the reaction. The organic phase was extracted with petroleum ether, washed with saturated sodium chloride solution, and then washed three times with deionized water. The organic phase was dried over anhydrous magnesium sulfate and filtered. The filtrate was concentrated by rotary evaporation under reduced pressure to give Compound 1 as a pale yellow oil (2.13 g). The product was used directly in the polymerization without further purification.

(2) Synthesis method of (3-octyl-2-thienyl) tributylstannane

Under review

(Compound 2)[31]

Under a N_2 atmosphere, 3-octylthiophene (0.294 g, 1.5 mmol) was dissolved in 25 mL of super-dry THF in a 100 mL two-necked flask and then cooled to -78 °C. A 2.5 mol/L solution of n-BuLi in hexane (0.6 mL, 1.5 mmol) was added dropwise. After the addition was complete, the mixture was allowed to warm to 0 °C and stirred for 1 h, then cooled again to -78 °C. Tributyltin chloride (0.538 g, 1.65 mmol) was added dropwise, and the mixture was stirred overnight. After the reaction, an appropriate amount of deionized water was added to quench the reaction. The organic phase was extracted with petroleum ether, then washed three times with deionized water, dried over anhydrous magnesium sulfate, and filtered. The filtrate was concentrated by rotary evaporation under reduced pressure to give Compound 2 as a pale yellow oil (0.74 g). The product was used directly in the next step without further purification.

(3) Synthesis method of 5, 6-difluoro-4, 7-bis (4-octyl-2-thienyl) -benzothiadiazole (Compound 3)[32]

Under a N_2 atmosphere, 4, 7-dibromo-5, 6-difluorobenzothiadiazole (0.111 g, 0.335 mmol), Compound 2 (0.406 g, 0.838 mmol), and tetrakis (triphenylphosphine) palladium (0) (19.4 mg, 5 mol%) were dissolved in 12 mL of super-dry THF in a 50 mL round-bottom flask. The mixture was stirred under reflux for 24 h. After the reaction mixture was cooled to room temperature, an appropriate amount of deionized water was added to quench the reaction. The organic phase was extracted with dichloromethane, then washed three times with deionized water, dried over anhydrous magnesium sulfate, and filtered. The filtrate was concentrated by rotary evaporation under reduced pressure, and the residue was purified by column chromatography using petroleum ether/dichloromethane (4:1) as the eluent to obtain Compound 3 as a yellow powder (0.128 g, yield 68%). ^{1}H NMR (500 MHz, Chloroform - d) δ = 8.11 (s, 2H), 7.20 (s, 2H), 2.71 (t, J = 7.7 Hz, 4H), 1.70 (m, 4H), 1.37-1.23 (m, 20 H), 0.88 (t, J = 6.7 Hz, 6H).

(4) Synthesis method of FBT-ThC$_8$-Br[32]

Compound 3 (86 mg, 0.153 mmol) and N-bromosuccinimide (NBS) (68.22 mg, 0.382 mmol, 2.5 eq) were dissolved in 10 mL of super-dry THF in a 50 mL round-bottom flask, followed by the addition of three drops of glacial acetic acid. The reaction mixture was stirred under dark conditions for 12 h. After the reaction was complete, deionized water was added to quench the reaction. The organic phase was extracted with dichloromethane, then washed three times with deionized water, dried over anhydrous magnesium sulfate, and filtered. The filtrate was concentrated by rotary evaporation under reduced pressure, and the residue was purified by column chromatography using petroleum ether/dichloromethane (3:1) as the eluent to obtain Compound 4 as an orange powder (91 mg, yield 82%). ^{1}H NMR (500 MHz, Chloroform - d) δ = 7.93 (s, 2H), 2.64 (t, J = 7.7 Hz, 4H), 1.66 (m, 4H), 1.40 - 1.21 (m, 20H), 0.89 (t, J = 6.8Hz, 6H).

(5) Synthesis method of 4, 7-bis (4-octyl-2-thienyl) -benzothiadiazole (Compound 4)[32]

Under a N_2 atmosphere, 4, 7-dibromobenzothiadiazole (0.127 g, 0.433 mmol), Compound 2 (0.462 g, 0.952 mmol), and tetrakis (triphenylphosphine) palladium (0) (25 mg, 5 mol%) were dissolved in 12 mL of super-dry THF in a 50 mL round-bottom flask. The synthesis method was adapted from that of Compound 3, using petroleum ether/dichloromethane (5:1) as the eluent, to obtain Compound 5 as a yellow powder (0.161 g, yield 71%). ^{1}H NMR (500 MHz, Chloroform - d) δ = 7.96 (s, 2H), 7.80 (d, J = 3.7 Hz, 2H), 7.03 (s, 2H), 2.68 (t, J = 7.8 Hz, 4H), 1.70 (m, 4H), 1.40 - 1.25 (m, 20H), 0.88 (t, J = 6.6Hz, 6H).

(6) Synthesis method of BT-ThC$_8$-Br[32]

Compound 4 (100 mg, 0.190 mmol) and N-bromosuccinimide (NBS) (84 mg, 0.475 mmol, 2.5 eq) were dissolved in 10 mL of super-dry THF in a 50 mL round-bottom flask. The synthesis method was adapted from that of Compound 4, using petroleum ether/dichloromethane (4:1) as the eluent, to obtain Compound 6 as a bright yellow powder (0.104 g, yield 80%). ^{1}H NMR (500 MHz, Chloroform - d) δ = 7.75 (s, 2H), 7.72 (s, 2H), 2.63 (t, J = 7.8 Hz, 4H), 1.66 (m, 4H), 1.39 - 1.27 (m, 20H), 0.88 (t, J = 6.6Hz, 6H).

(7) The synthesis method of PFBT is as follows[32]

Under a N_2 atmosphere, FBT-ThC$_8$-Br (60 mg, 0.083 mmol) was dissolved in 8 mL of toluene in a 50 mL round-bottom flask. Then, Compound 1 (61 mg, 0.092 mmol) and tetrakis (triphenylphosphine) palladium (0) (4.7 mg, 5 mol%) were added. The mixture was stirred under reflux for 24 h. After the reaction was complete and the mixture was cooled to room temperature, the reaction solution was poured into methanol to precipitate the solid, which was then collected by filtration. The filter cake was washed successively with methanol, petroleum ether, and dichloromethane, and then dried under vacuum for 12 h to obtain PFBT as a dark purple powder (60 mg, yield 49%).

(8) The synthesis method of PBT is as follows[32]

Under a N_2 atmosphere, BT-ThC$_8$-Br (56 mg, 0.082 mmol), Compound 1 (59 mg, 0.089 mmol), and tetrakis (triphenylphosphine) palladium (0) (4.7 mg, 5 mol%) were dissolved in 8 mL of toluene in a 50 mL round-bottom flask. The synthesis method was adapted from that of PFBT to obtain PBT as a dark purple powder (60 mg, yield 52%).

The details of the characterization, photocatalytic reactions, photoelectrochemical measurements, theoretical calculations, and NMR data are provided in Supporting Information.

Just Accepted

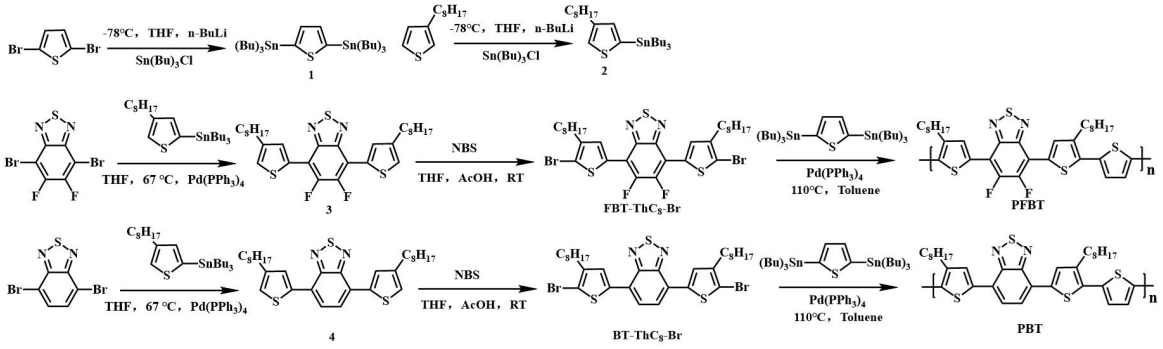


Fig. 1 Synthetic routes of PFBT and PBT.

3. Results and Discussion

3.1 Characterization of Film-PBT and Film-PFBT

The synthesis procedures of the two conjugated polymers, PBT and PFBT (whose molecular structures are shown in Fig. 2(a, b)). To further confirm the successful synthesis of the target products PFBT and PBT, Fourier-transform infrared spectroscopy (FT-IR) analysis was performed on the reaction monomers and the resulting polymers. As presented in Fig. S1, the C-Br stretching vibration band at 628 cm^{-1} was observed for the monomers FBT-ThC8-Br and BT-ThC8-Br. Notably, this characteristic absorption peak was found to be completely absent in the spectra of PFBT and PBT, confirming the successful polymerization of the monomers through the Stille cross-coupling reaction. Additionally, XPS survey spectra were acquired to verify the elemental composition of PBT and PFBT polymers. As shown in Fig. S2, characteristic signals of C 1s, N 1s, S 2s and S 2p can be detected in both polymers, matching their expected elemental composition. A distinct F 1s peak at ~688 eV is observed in the survey spectrum of PFBT, while no F 1s signal is present in PBT, directly confirming the successful incorporation of fluorine atoms into the PFBT backbone. Combined with the FT-IR results, the XPS survey data further validate the successful synthesis of PBT and PFBT. The high-resolution C 1s spectra of PBT and PFBT were further deconvoluted to analyze the local chemical environments of carbon atomsa (Fig. S3). For PBT, three carbon components were fitted: C–C/C=C at 284.8 eV, C–S at 285.7 eV, and C=N/C–N at 286.5 eV. For PFBT, an additional peak at ~288.0 eV assigned to aromatic C–F bond was clearly resolved, which further evidences the introduction of fluorine substituents on the polymer backbone. Thermal stability constitutes a critical parameter in assessing the practical viability of materials for real-world applications[33]. As can be observed in Fig. S4, the 5% decomposition temperatures of PFBT and PBT were determined to be 430 °C and 454 °C, respectively. The results indicated that the introduction of fluorine atom onto the BT skeleton would increase the thermal stability of the corresponding copolymers. Subsequently, the thin-film materials were prepared as follows. As shown in Fig. S5, 20 mg of PFBT and 20 mg of PBT were weighed and transferred into two separate 5 mL brown reagent bottles, respectively. Then, 1 mL of chlorobenzene was added to each bottle using a pipette, and the mixtures were ultrasonically dissolved. Subsequently, 1 mL of each solution was taken and uniformly coated onto glass slides with a side length of 2.5 cm. After the chlorobenzene had naturally evaporated, black thin-film materials were obtained (with a photocatalyst loading of 2 mg). To investigate the morphology of the polymer thin films, microscopic images of the film materials were obtained using an industrial camera under 50 magnification (Fig. 2c). It can be observed that the materials are uniformly loaded on the glass slide surface with a homogeneous texture. To gain a deeper understanding of the surface morphology of the thin film, atomic force microscopy measurements were performed on a 5 × 5 μm^2 area of the film (Fig. 2(d-g). The Film-PBT and Film-PFBT films displayed a relatively smooth surface with average root mean square (RMS) roughness values of 1.98nm and 1.65 nm, respectively. The smoother surface indicating that the films possess fewer defect sites, leading to improved charge separation and transport, thereby enhancing the photocatalytic removal of uranium. To further investigate the crystalline nature and molecular orientation, thin films and powders of these polymers were also characterized by X-ray diffraction (XRD). The polymer powders and their thin films spin-coated onto ITO glass substrates were characterized by X-ray diffraction (XRD). The XRD pattern of the bare ITO glass substrate was also recorded as a reference to exclude interference from diffraction signals originating from the substrate. As shown in Fig. 2(h), both the thin films and powders exhibit a low-intensity (010) diffraction peak at around 25°, which is related to the π-π stacking distances (dπ) between coplanar conjugated polymers. The (010) diffraction angles were calculated to be approximately 23.84°, 25.15°, 25.07°, and 25.25°, and the corresponding dπ distances were evaluated to be 3.73 Å for PBT, 3.55 Å for Film-PBT, 3.54 Å for PFBT, and 3.55 Å for Film-PFBT, respectively. Compared with the powders, all films displayed additional diffraction peaks in the range of 5-15°, which are related to the lamellar spacings (dl) between coplanar conjugated polymers. Specifically, the peaks at 5.36° and 5.76° correspond to the (100) reflection, and those at 11.64° and 11.55° correspond to the (200) reflection. From the XRD patterns, Film-PFBT exhibits a higher (100) peak intensity than Film-PBT, indicating higher crystallinity. The lamellar spacings (dl) were calculated to be 1.65 Å for Film-PBT (from 5.36°) and 1.53 Å for Film-PFBT (from 5.76°). Therefore, the introduction of fluorine atoms reduces the lamellar spacings. It is worth noting that both polymer films exhibit a relatively strong peak at 12.51°, which may correspond to another ordered packing scale perpendicular to the side-chain stacking direction, further indicating that the films have more ordered packing compared to

Just Accepted

the powders. Through comprehensive consideration of the XRD results, the copolymer film is more favorable for ordered molecular packing. In particular, the fluorinated copolymer film exhibits a more regular interchain arrangement of polymer molecules, which will enhance the charge transport capability of the material[34, 35].

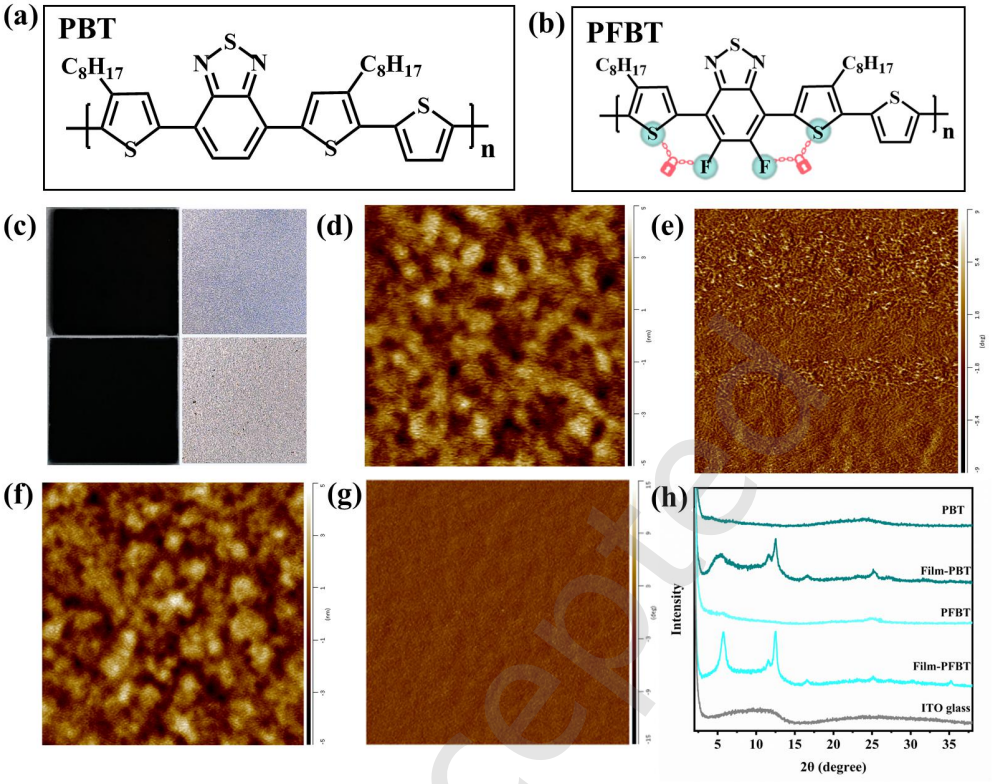


Fig. 2 Schematic structures of PBT and PFBT (a , b); Photographs of Film-PBT and Film-PFBT (upper left, lower left) ; Images of Film-PBT and Film-PFBT under 50× zoom (upper right, lower right) (c); AFM height images and phase images of the film. Film-PBT (d, e) Film-PFBT (f, g); Image size: 5 × 5 μm^2 ; X-ray diffraction (XRD) patterns of PBT, Film-PBT, PFBT, Film-PFBT and ITO glass (h).

3.2 Photoelectric Properties and Charge Carrier Dynamics

To investigate the light absorption performance of the polymers, UV-vis absorption spectra were recorded using a UV-vis spectrophotometer over the wavelength range of 350-1000 nm, as displayed in Fig. 3(a). The results reveal that PFBT exhibits a remarkable red-shift in the maximum absorption wavelength and a broader absorption spectrum compared with PBT. This may be ascribed to the incorporation of fluorine atoms that generate intramolecular non-covalent conformational locks, enhancing molecular planarity and thus extending the light absorption range[36]. Notably, after film formation, both materials exhibited a red shift in light absorption, with the absorption range covering the entire visible region and a significant enhancement in light-harvesting capability. This indicates that the ordered arrangement of polymer molecular chains during the film-formation process improves the optical absorption performance of the materials20. According to the Tauc plot analysis, the bandgap values of PBT, Film-PBT, PFBT, and Film-PFBT were determined to be 1.64 eV, 1.82 eV, 1.52 eV, and 1.58 eV, respectively (Fig. 3(b-c)). It can be seen that both fluorination and film formation lead to a reduction in the bandgap, which will generate more photogenerated charge carriers and thereby enhance the photocatalytic activity. To further characterize the band structures of Film-PBT and Film-PFBT, Mott-Schottky measurements were performed (Fig. 3(d-e)). The slopes of the tangent lines in the Mott-Schottky plots are positive for both samples, indicating that both Film-PBT and Film-PFBT are n-type semiconductors. Their flat-band potentials were determined to be -1.14 V and -0.93 V, respectively, from which the LUMO energy levels were calculated to be -0.94 V and -0.73 V, respectively. According to the bandgap formula ($E_g = E_{CB} - E_{VB}$)[37], the HOMO energy levels of the two materials were thus determined to be 0.70 V and 0.79 V, respectively, from which the band alignment diagrams of the two materials were plotted as shown in Fig. 3(f). It can be seen that fluorination-mediated modulation of the electron acceptor unit can serve as an effective strategy for optimizing the redox potentials of D-A type materials.Subsequently, the photogenerated charge separation and migration capabilities of Film-PBT and Film-PFBT were investigated using transient photocurrent response and electrochemical impedance spectroscopy. As shown in Fig. 3(g), the photocurrent density of Film-PFBT under illumination was

Just Accepted

higher than that of Film-PBT, indicating that the introduction of fluorine atoms into the benzothiadiazole unit can improve the separation efficiency of photogenerated electrons and holes, thereby enabling more photogenerated electrons to participate in the photocatalytic reaction and enhancing the photocatalytic activity. Fig. 3(h) shows the electrochemical impedance spectra of the two materials. It can be seen that the arc radius of Film-PFBT is smaller than that of Film-PBT, indicating that, owing to the electron-withdrawing effect of fluorine atoms, Film-PFBT possesses lower charge transfer resistance and faster interfacial charge migration capability[38]. To understand the photogenerated charge recombination behavior of Film-PFBT and Film-PBT, their photoluminescence (PL) spectra were measured (Fig. 3i). Under excitation at 500 nm, the fluorescence intensity of Film-PFBT was weaker than that of Film-PBT, indicating that the recombination of photogenerated electrons and holes in Film-PFBT was significantly suppressed[39].

In conclusion, the fluorination-based modulation of the electron-acceptor moiety serves to enhance the optical absorption capability, optimize the redox potentials, facilitate photogenerated carrier separation and charge transport, and effectively suppress charge recombination in the photocatalyst system.

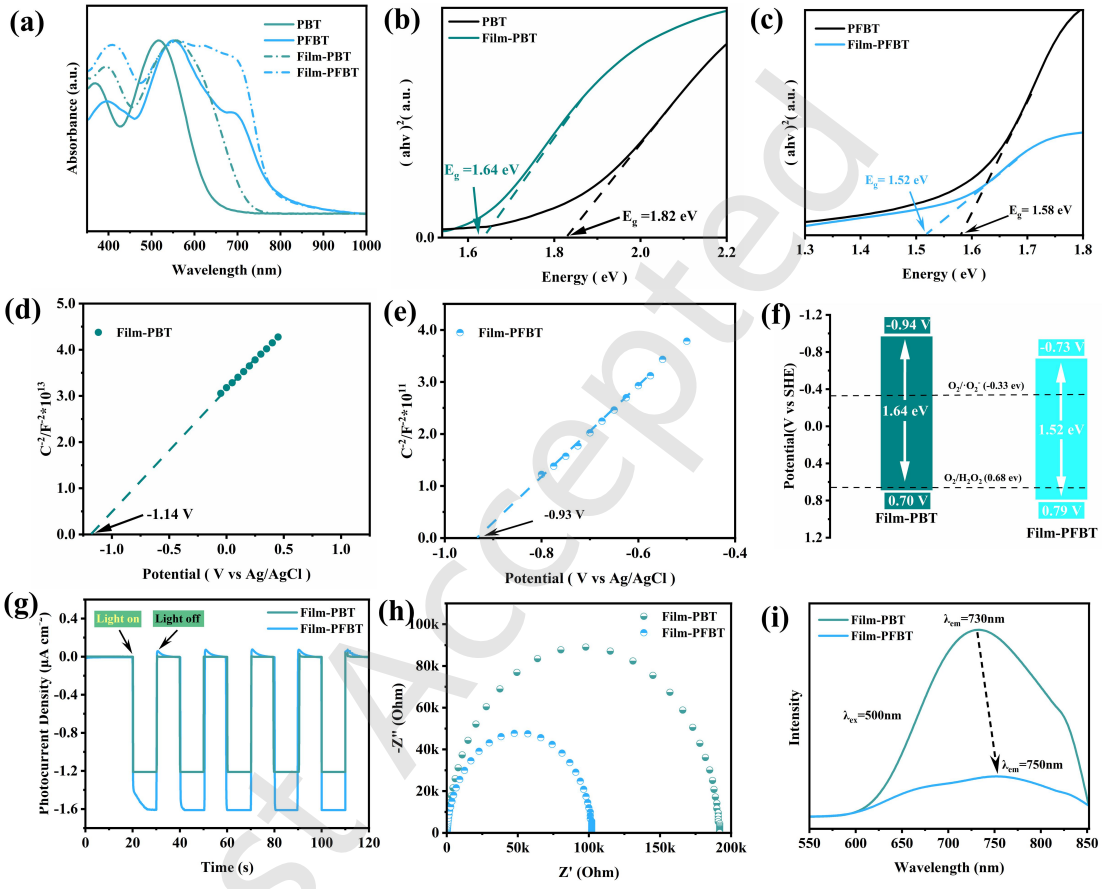


Fig. 3 UV-visible absorption spectra of PBT, PFBT, Film-PBT, and Film-PFBT (a); Tauc of PBT and Film-PBT(b); Tauc of PFBT and Film-PFBT (c); Mott-Schottky plots of Film-PBT (d) and Film-PFBT (e); Band diagram of Film-PBT and Film-PFBT (f); Transient photocurrent response spectra of Film-PBT and Film-PFBT (g); Electrochemical impedance spectra (EIS) of Film-PBT and Film-PFBT (h); Photoluminescence (PL) spectra of Film-PBT and Film-PFBT (i).

3.3Photocatalytic Uranium (VI) Removal Performance of Film-PBT and Film-PFBT

In a photocatalytic system for U(VI) removal, the hole scavenger and the pH of the UO_2^{2+} aqueous solution are two critical parameters that require optimization to maximize the photocatalyst's removal efficiency. Photocatalytic experiments were conducted under the following conditions: pH = 5, solution volume of 50 mL, and initial UO_2^{2+} concentration of 50 ppm. Three different hole scavengers methanol (MeOH), isopropanol (IPA), and ethanol (EtOH) were respectively employed to evaluate the U(VI) removal performance of Film-PFBT and Film-PBT (Fig. 4a; Fig. S6). As clearly shown in Fig. 4a and Fig. S6, both film photocatalysts achieved the highest removal efficiency when methanol was used as the hole scavenger. After determining the appropriate hole scavenger, the optimal pH value of the UO_2^{2+} solution was investigated (Fig. 4b). It was found that when the pH of the UO_2^{2+} solution increased from 3 to 7 (under 4 h of illumination), the removal efficiencies of both Film-PFBT and Film-PBT exhibited a trend of first increasing and then decreasing, with both showing the best removal performance at pH = 5. Furthermore, Film-PFBT achieved removal efficiencies above 80% at pH values of 4, 5, and 6, demonstrating good pH adaptability.

Under the conditions of pH = 5, a solution volume of 50 mL, a UO_2^{2+} concentration of 50 ppm, and the addition of 2 mL of methanol, the photocatalytic U(VI) removal performances of powder PBT, powder PFBT, Film-PBT and Film-PFBT were systematically compared (Fig. 4c). A 60 min dark adsorption process was implemented prior to visible light irradiation to

Just Accepted

achieve adsorption-desorption equilibrium. At 300 min, the powder PBT and powder PFBT achieved U (VI) removal efficiencies of 73.4% and 86.2%, respectively. In sharp contrast, Film-PBT and Film-PFBT delivered much higher removal efficiencies of 87.0% and 95.1%. Compared with Film-PBT, Film-PFBT exhibited superior photocatalytic U(VI) removal performance, achieving approximately 95% removal efficiency for UO_2^{2+} after 4 h of illumination, following a 60 min adsorption-desorption equilibrium period in the dark. From the pseudo-first-order kinetic curves (Fig. 4d), the rate constants for Film-PFBT and Film-PBT were determined to be 0.01435 min^{-1} and 0.00824 min^{-1}, respectively. The larger rate constant of Film-PFBT indicates a faster removal rate in the photocatalytic U(VI) reduction process.This is because the fluorine atoms reduce the dihedral angles of the molecular backbone by forming non-covalent conformational locks, thereby improving the planarity of the framework. As a result, the transport efficiency of photogenerated charge carriers is effectively enhanced and the recombination rate is reduced, which facilitates the participation of more photogenerated electrons in the photocatalytic reaction of U(VI).

The reusability and anti-ion interference capability of materials are critically important for practical applications. In the reusability tests, after each photocatalytic reaction (4 h of illumination per cycle), the films were immersed in 0.2 mol/L Na_2CO_3 solution for 6 h to remove the deposited uranium oxides from the film surface. It was found that Film-PFBT maintained nearly 90% removal efficiency after four cycles of photocatalytic U(VI) removal tests (Fig. 4e), indicating that Film-PFBT possesses good stability and excellent photocatalytic U(VI) removal capability. The XRD patterns of the original Film-PFBT and the sample after adsorption-desorption cycles are shown in Fig. S7. It can be observed that the position of characteristic diffraction peaks remains nearly unchanged after repeated adsorption-desorption cycling. No new impurity peaks appear, demonstrating that the crystalline structure of Film-PFBT is well maintained and the material possesses good structural stability during the cycling process. In addition, considering that real uranium mine wastewater often contains abundant metal cations, the selectivity of Film-PFBT toward UO_2^{2+} was evaluated. Photocatalytic U(VI) removal tests were conducted in UO_2^{2+} solutions containing Na^+, K^+, Mg^{2+}, Co^{2+}, Ni^{2+}, Zn^{2+}, and VO_2^+ ions (with a mass concentration ratio of M^{n+} : UO_2^{2+} = 50:1) (Fig. 4f). The results showed that, except for VO_2^+, which has a similar coordination mode to UO_2^{2+}, Film-PFBT maintained a removal efficiency of approximately 90% even in the presence of other interfering cations, demonstrating its excellent anti-interference capability. As listed in Supporting Information Table 1, we also investigated the U(VI) removal performance of various recently reported materials under their respective optimal pH conditions. These features highlight its great potential for U(VI) remediation[40-45]. Fig. 4(g) shows a photograph of the Film-PFBT thin film used in the experiment, providing a visual representation of the appearance and morphology of the prepared black film sample. It is accompanied by a photograph of the photocatalytic reaction setup, clearly illustrating the reaction channel, light source system, peristaltic pump, and liquid storage unit, thereby fully presenting the operational system for the dynamic photocatalytic removal of U(VI). To evaluate the feasibility of Film-PFBT for practical applications, this study employed raw uranium mine wastewater as the test medium. The wastewater is characterized by typical high salinity and a complex matrix, with a total dissolved solids (TDS) content as high as 2500 $mg \cdot L^{-1}$ and the presence of a large number of competing ions. The specific water quality conditions are as follows: the initial concentration of hexavalent uranium (U(VI)) is 160.4 $mg \cdot L^{-1}$, among the major coexisting ions, the sodium ion concentration is 1680 $mg \cdot L^{-1}$, sulfate ion concentration is 1490 $mg \cdot L^{-1}$, and carbonate ion concentration is 450 $mg \cdot L^{-1}$. Under such high-salinity, high-interference real wastewater conditions, Film-PFBT still exhibited satisfactory treatment performance toward the target contaminant, achieving a U(VI) removal efficiency of over 60%. This verifies its selective adsorption capability for U(VI) in complex matrices and its potential application value (Fig. 4h).

Just Accepted

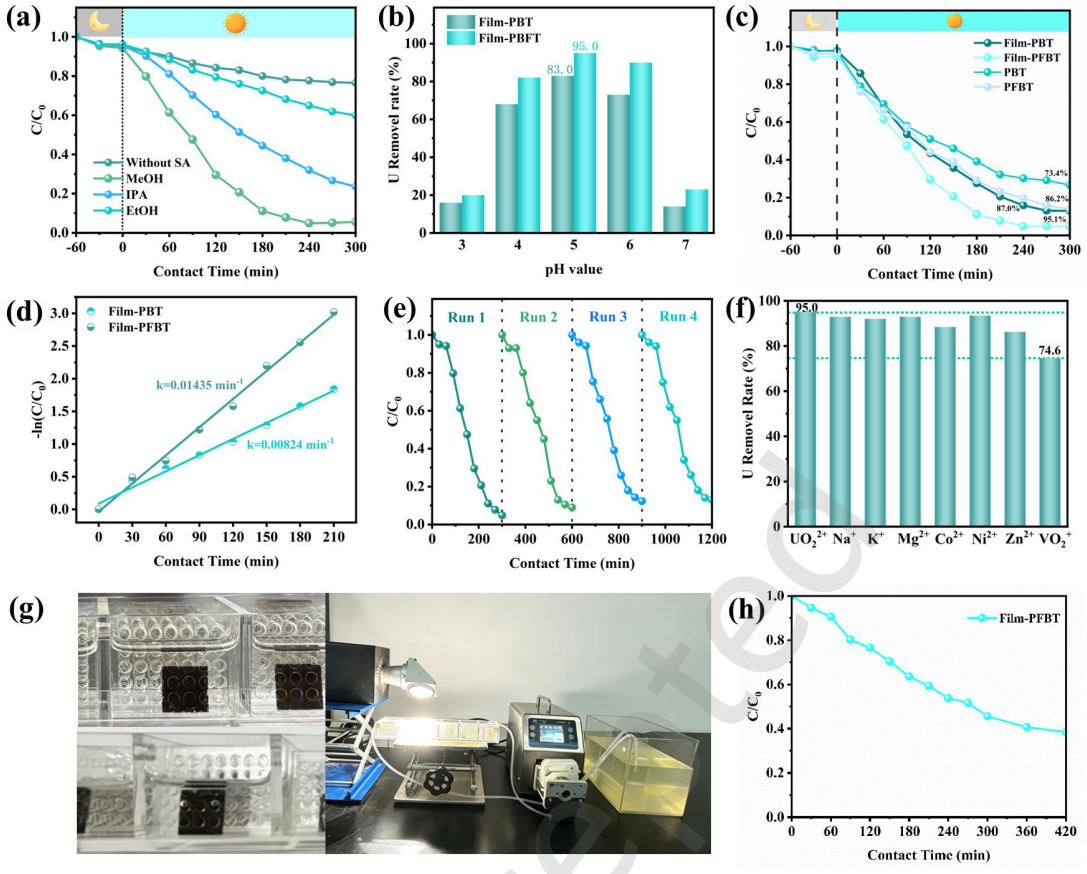


Fig. 4 Photocatalytic U(VI) removal performance curves of Film-PFBT using different sacrificial agents (a); Photocatalytic U(VI) removal performance at different pH values of UO_2^{2+} solution (b); Comparison curves of photocatalytic U(VI) removal performance of powder PBT, powder PFBT, Film-PBT and Film-PFBT (c); Pseudo-first-order kinetic plots of Film-PBT and Film-PFBT (d); Cyclic tests of photocatalytic U(VI) removal for Film-PFBT (e); Anti-ion interference experiment (f); Optical photograph of the black polymer film on glass and schematic diagram of photocatalytic device (g); Photocatalytic efficiency of Film-PFBT in natural uranium mine wastewater (h).

3.4 Density Functional Theory (DFT) Calculations

To explore the modulating effect of fluorination on the conformation of conjugated polymers, we calculated the optimized molecular geometries and key dihedral angles of PBT and PFBT using density functional theory (DFT). As shown in Fig. 5(a-b), and Table S2, the dihedral angles between the BT unit and adjacent thiophene units in the PBT backbone (θ_1 = 0.32° and θ_2 = 6.08°) and the dihedral angle between the terminal thiophene units (θ_3 = 44.34°) reveal significant conformational distortion. In contrast, for the fluorinated PFBT, non-covalent conformational locking interactions were formed between the F atoms and the S atoms of the adjacent thiophene units[46], the F···S atomic distances were determined to be 2.730 Å and 2.736 Å (Fig. 5(c)), which are smaller than their theoretical van der Waals distance of 2.99 Å. As a result, θ_1 and θ_2 were significantly reduced to 0.21° and 0.91°, respectively, while θ_3 was simultaneously decreased to 30.99°, indicating a substantial improvement in the planarity of the molecular backbone. This conformational planarization effectively enhances the π-π stacking interactions between molecular chains, providing a structural basis for improving the optoelectronic properties of the material[47, 48]. This conformational regulation offers multiple advantages. First, the planarized molecular conformation can effectively reduce steric hindrance between conjugated chains, promoting ordered packing of molecular chains. Second, the enhanced π-π interactions can improve charge carrier mobility while broadening the light absorption range of the material[48]; In addition, the conformational lock effect can enhance the conformational stability of the polymer in both solution and thin-film states, reduce defect sites, and provide favorable conditions for charge separation and transport during the photocatalytic process[49].

To conduct an in-depth investigation into the band structures of the two conjugated polymers, DFT calculations were systematically employed to study the intramolecular excited-state electron transfer process of the photocatalysts. The frontier molecular orbital distributions of polymer chain segment are shown in Fig. 5d. The HOMO energy levels of both materials are primarily localized on the thiophene groups (D), while the LUMO energy levels are highly delocalized over the difluorobenzothiadiazole and benzothiadiazole acceptor groups (A). This indicates that photogenerated electrons can rapidly transfer along the polymer chain from the thiophene groups to the difluorobenzothiadiazole and benzothiadiazole acceptor groups, enabling efficient separation of photogenerated electron–hole pairs[50]. The calculation results show that LUMO energy levels of PFBT and PBT were -2.72 eV and -2.62 eV (vs. vacuum), respectively, and the HOMO energy levels were -5.12 eV and -5.98 eV (vs. vacuum), respectively. The introduction of

Just Accepted

fluorine atoms lowered both the LUMO and HOMO energy levels of the materials, which is consistent with the experimental results.

In donor-acceptor (D-A) systems, due to the difference in electron affinity between the donor (D) and acceptor (A) units, an internal electric field is formed within the molecule. The strength of this internal electric field affects the degree of photogenerated charge carrier separation, and the molecular dipole moment serves as an important criterion for evaluating the intensity of the internal electric field[51]. From the molecular electrostatic potential (ESP) maps (Fig. 5e), it can be observed that the degree of positive and negative charge separation in PFBT is significantly higher than that in PBT. This difference results in a larger dipole moment for PFBT. The computational results further confirm this trend, with PFBT exhibiting a dipole moment of 1.3361 Debye, while PBT has a dipole moment of 0.6012 Debye. A larger dipole moment generally implies a stronger built-in electric field, which facilitates rapid separation of photogenerated charge carriers and thereby enhances photocatalytic activity.

The construction of planar and continuous π-electron delocalization channels can promote the transport of photogenerated charges. To study the π-electron delocalization channels of PFBT and PBT, simulations were performed on their oligomer chain fragments. As shown in Fig. 5f, the red and orange pathways indicate that both PFBT and PBT exhibit highly delocalized π-electrons. The planar and continuous π-electron delocalization channels formed by the thiophene and benzene rings endow the materials with a highly extended π-conjugated backbone, which facilitates the transport of photogenerated charges and thus enhances photocatalytic activity[52].

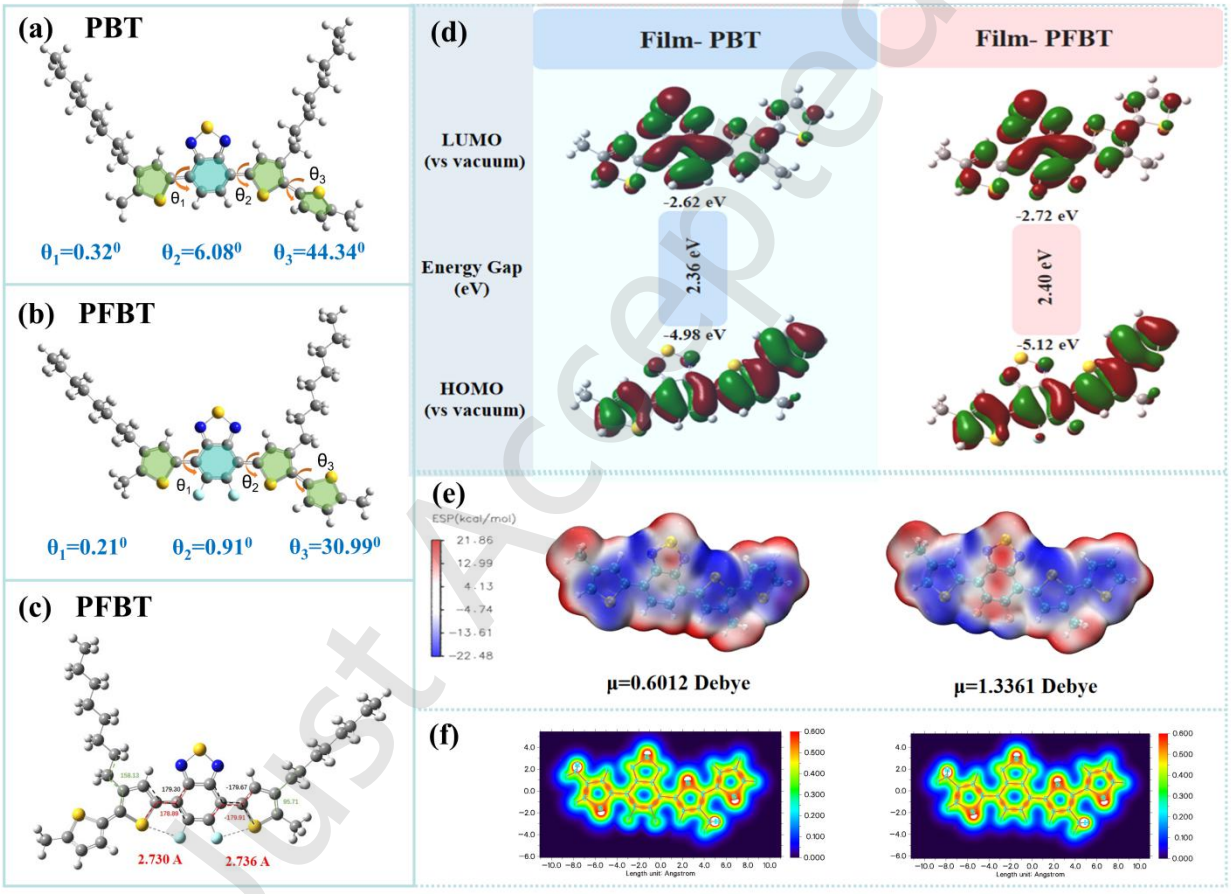


Fig. 5 Ball-and-stick model and schematic diagram of the key dihedral angle of PBT(a); Ball-and-stick model and schematic diagram of the key dihedral angle of PFBT(b); The structure of PFBT with labeled intramolecular F···S distances and dihedral angles (c); HOMO and LUMO orbital distributions of polymer fragments obtained from DFT simulations (d); Electrostatic surface potential and dipole moment (e); LOL-π electron delocalization above the Bohr radius (f).

3.5 Mechanism of Photocatalytic Uranium (VI) Removal by Film-PFBT

To investigate the reaction mechanism of photocatalytic U(VI) removal by Film-PFBT, X-ray photoelectron spectroscopy (XPS) analysis was performed on the Film-PFBT samples. Compared with the pristine Film-PFBT sample, a new U 4f signal peak appeared in the survey XPS spectrum of Film-PFBT after photocatalytic U(VI) removal (Fig. 6a), indicating the successful progress of the photocatalytic U(VI) removal process. Subsequently, the high-resolution U 4f spectrum was analyzed. As shown in Fig. 6b, two strong peaks were attributed to U(VI) $4f_{5/2}$ (392.96 eV) and U(VI) $4f_{7/2}$ (393.25 eV), respectively, confirming that the uranium oxides generated after the photocatalytic reaction of Film-PFBT are hexavalent uranium. Notably, in the high-resolution N 1s spectrum, the peak corresponding to C=N-S (399.40 eV) shifted to a higher binding energy by 0.14 eV after photocatalytic U(VI) removal (Fig. S8), indicating that electrons in the vicinity of the thiadiazole unit of the benzothiadiazole moiety participated in the photocatalytic reaction. To further investigate the morphology of the uranium

Just Accepted

oxides after the photocatalytic reaction, X-ray diffraction (XRD) analysis was performed on the sample after photocatalysis. As shown in Fig. 6c, compared with the pristine sample, the XRD pattern of Film-PFBT after the photocatalytic reaction exhibited new diffraction peaks at 16.96°, 20.22°, 23.34°, 25.04°, 27.38°, 32.48°, 33.56°, 36.36°, and 37.34°, which are in full agreement with the diffraction peaks of $(UO_2)O_2•2H_2O$[53].

Investigating the reactive species involved in the photocatalytic reaction is crucial for elucidating the reaction mechanism. To explore the active species participating in the photocatalytic U(VI) removal by Film-PFBT, radical trapping experiments were conducted to study the effects of h^+, e^-, $·O_2^-$, and ·OH on the photocatalytic reaction. Methanol (MeOH), potassium bromate ($KBrO_3$), p-benzoquinone (p-BQ), and tert-butanol (TBA) were used as scavengers for h^+, e^-, $·O_2^-$, and ·OH, respectively. As shown in Fig. 6d, the photocatalytic U(VI) removal efficiency of Film-PFBT was significantly enhanced in the presence of methanol. This is because methanol, acting as a hole (h^+) scavenger, reacts with photogenerated holes, thereby reducing the recombination rate of photogenerated electrons and holes and allowing more photogenerated electrons to participate in the photocatalytic reaction. The addition of potassium bromate and p-benzoquinone had a marked influence on the photocatalytic U(VI) removal performance of Film-PFBT, especially in the presence of p-benzoquinone. This indicates that e- and $·O_2^-$ are the most dominant reactive species in the photocatalytic U(VI) removal process. In contrast, when tert-butanol was present in the UO_2^{2+} solution, its effect on the photocatalytic U(VI) removal was almost negligible.

To further confirm the presence or absence of $·O_2^-$ and ·OH during the photocatalytic process, radical trapping experiments were conducted. Nitro blue tetrazolium chloride (NBT) and coumarin were used as trapping agents for $·O_2^-$ and ·OH, respectively. As shown in Fig. S9, the absorbance of NBT decreased with increasing irradiation time, demonstrating that a large amount of $·O_2^-$ was generated and participated in the photocatalytic U(VI) removal process. The coumarin fluorescence intensity experiment (Fig. S10) revealed that the fluorescence intensity remained almost unchanged with increasing irradiation time, indicating that Film-PFBT could not generate ·OH under light irradiation. The results of the radical trapping experiments were consistent with those of the radical quenching experiments.

Finally, electron paramagnetic resonance (EPR) spectroscopy was employed to further investigate whether e^- and $·O_2^-$ reactive species were generated by Film-PFBT under light irradiation. TEMPO was used as an electron-trapping agent, and DMPO was used as a superoxide radical-trapping agent. As shown in Fig. 6e, no characteristic DMPO-$·O_2^-$ signal was observed under dark conditions; however, upon light irradiation, a distinct DMPO-$·O_2^-$ signal was detected. Fig. 6f presents the characteristic curve of the electron-trapping agent TEMPO (which can be reduced to TEMPOH by electrons). It can be seen that the peak intensity under light irradiation was lower than that under dark conditions, indicating a decrease in TEMPO concentration. The EPR results further confirmed that both e^- and $·O_2^-$ reactive species were generated by Film-PFBT during the photocatalytic U(VI) removal process. In summary, the reactive species involved in the photocatalytic U(VI) removal by Film-PFBT are e^- and $·O_2^-$.

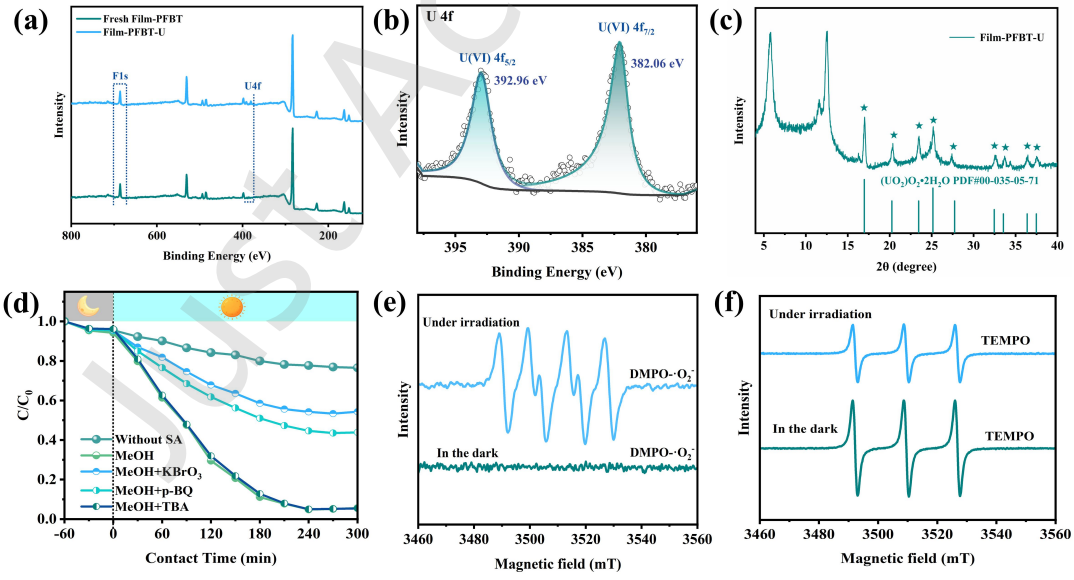


Fig. 6 XPS survey spectra of Film-PFBT before and after photocatalytic U(VI) removal (a); High-resolution U 4f XPS spectra of Film-PFBT after photocatalysis (b); XRD patterns of Film-PFBT after photocatalytic U(VI) removal (c); Radical quenching experimental curves of Film-PFBT (d); EPR spectra of DMPO-$·O_2^-$ under dark and light conditions (e); EPR spectra of TEMPO under dark and light conditions (f).

Previously, numerous literature reports have demonstrated that H_2O_2 can convert uranyl ions into $(UO_2)O_2•2H_2O$[53]. Based on this, the relationship between H2O2 concentration and irradiation time for Film-PFBT and Film-PBT under light irradiation was investigated using the iodometric method. As shown in Fig. S11, the concentration of H_2O_2 gradually increased with extended irradiation time, with the most rapid increase occurring within the first 30 min. The above results indicate that during the photocatalytic reaction, Film-PFBT can generate substantial amounts of H_2O_2, which subsequently reacts with uranyl ions to form $(UO_2)O_2•2H_2O$.

Just Accepted

In summary, a reasonable photocatalytic U(VI) removal mechanism for Film-PFBT is proposed. As illustrated in Fig. 7, upon light excitation, Film-PFBT generates photogenerated electrons and holes. Under the action of the built-in electric field, the electrons and holes are effectively separated, and the photogenerated electrons rapidly migrate to the difluorobenzothiadiazole units. The photogenerated holes are rapidly consumed by methanol to produce CO_2 and H_2O, while the photogenerated electrons are captured by oxygen to generate superoxide radicals ($\cdot O_2^-$), which further react to form H_2O_2. The generated H_2O_2 then reacts with UO_2^{2+} in the solution to form $(UO_2)O_2{\bullet}2H_2O$.

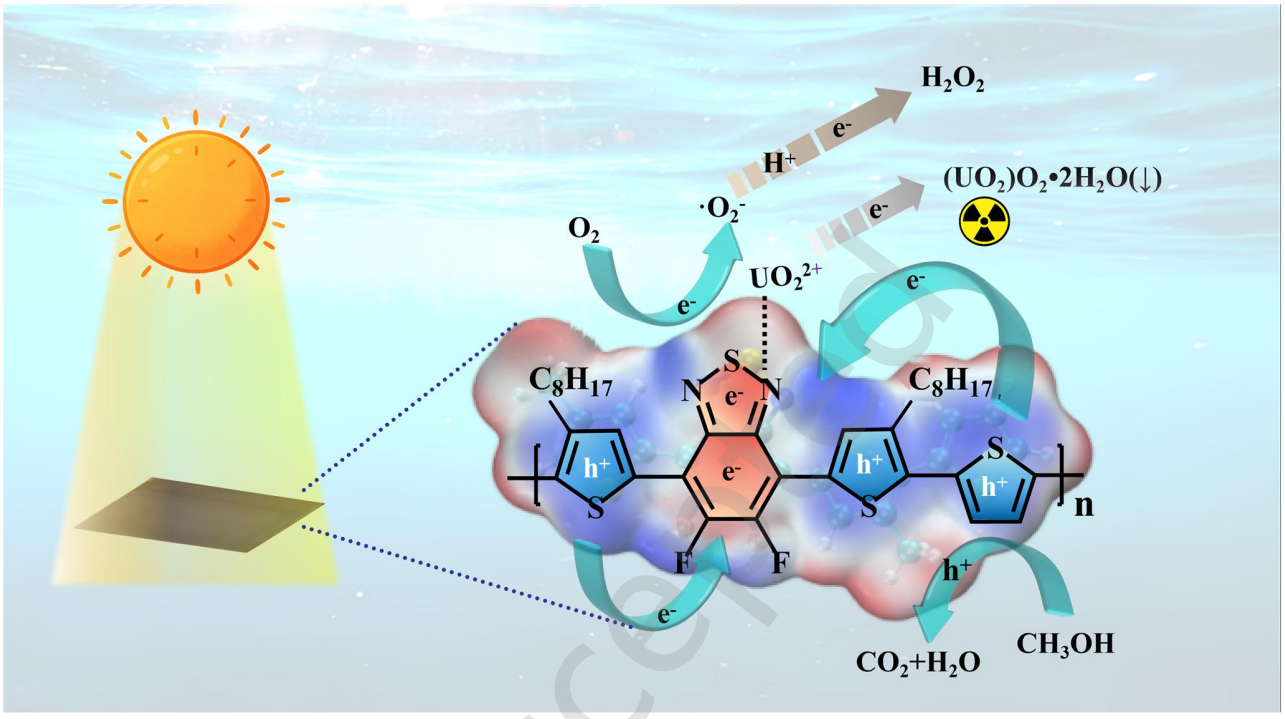


Fig.7 Schematic diagram of the photocatalytic U(VI) removal mechanism of Film-PFBT.

4. Conclusions

This study employs a fluorination regulation strategy to construct a conformational lock via F···S interactions, thereby enhancing the planarity of the material and improving its light absorption capability as well as photogenerated charge carrier transport. Meanwhile, the introduction of fluorine atoms strengthens the intramolecular built-in electric field, which promotes the separation efficiency of photogenerated charge carriers and the interfacial charge migration ability. Furthermore, thin-film fabrication techniques are further adopted to enhance the recyclability of the material in practical applications. This study provides a reference for the design of high-performance and recyclable D-A type photocatalysts.

Just Accepted

CRediT authorship contribution statement

Zuojia Li, Jinwei Shi: Writing-original draft, Investigation, Data curation. Hanting Wu: Software, Methodology, Yunhai Liu: Data curation, Funding acquisition. Zhibin Zhang, Yuanping Jiang: Writing-review & editing, Funding acquisition.

Declaration of competing interest

The authors declare that they have no known competing financial interests or personal relationships that could have appeared to influence the work reported in this paper.

Data availability

The data that support the findings of this study are available from the corresponding author upon reasonable request.

Acknowledgments

This study was financially supported by Key R&D Program of Jiangxi Province (No. 20243BBG71020), the National Natural Science Foundation of China (No. 22566004), the Natural Science Foundation of Jiangxi Province (Nos. 20252BAC240307, 20252BAC240309, 20242BAB20109). The authors extend their gratitude to Mr. Xin Wang (from Scientific Compass www.shiyanjia.com) for providing invaluable assistance with the EPR analysis.

Use of AI statement

None

Reference

[1] Jiang, Y.; Wang, F.; An, J.; Yu, X.; Cao, M.; He, G.; Xu, D.; Yang, J.; Zhang, K.; Zhang, Y.; Xu, L.; Li, Z.; Luo, X.; Zhang, Z.; Liu, Y. Flexible chain-engineered conjugated polymers with phosphonic acid anchors for synergistic photocatalysis-adsorption uranium extraction. Chem. Eng. J. 2025, 521, 166451.

[2] Li, Z.; Liu, X.; Chen, J.; Xu, D.; Li, Y.; Cao, M.; Zhu, Y.; Jiang, Y.; Zhang, Y.; Zhang, Z.; Liu, Y. Central metal-ion optimized photoconductive phthalocyanine polymers for efficient uranium removal. J. Environ. Chem. Eng. 2026, 14, 121992.

[3] Shi, J.; Fan, Q.; Zhu, Y.; Yang, J.; Li, Z.; Wu, H.; Zeng, X.; Xu, D.; Jiang, Y.; Zhang, Y.; Zhang, Z.; Liu, Y. Modulating photogenerated electron transfer by highly conductive EDOT π-bridge for efficient uranium extraction from water. Appl. Surf. Sci. 2026, 736, 166780.

[4] Bao, Y.-Y.; Liang, R.-P.; Jiang, Q.-Q.; Wang, X.; Zhang, Z.-W.; Zhang, C.-R.; Yu, F.-T.; Qiu, J.-D. Structural asymmetry induced built-in electric field enhancement for efficient photocatalytic uranium removal. Sep. Purif. Technol. 2026, 395, 137738.

[5] Zhang, W.; Deng, X.; Zhu, Y.; Yang, H.; Yu, F.; Liu, C. Breaking symmetry of active sites to enable long-lived shallow trapping in COFs for photocatalytic remediation of uranium-contaminated wastewater. Chem. Eng. J. 2026, 534, 175001.

[6] Niu, C.-P.; Zhang, C.-R.; Liu, X.; Liang, R.-P.; Qiu, J.-D. Synthesis of propenone-linked covalent organic frameworks via Claisen-Schmidt reaction for photocatalytic removal of uranium. Nat. Commun. 2023, 14, 4420.

[7] Luan, T. X.; Wei, Q.; Xin, C.; Wong, S. Y.; Li, Y.; Zheng, Y.; Li, Y.; Liu, G.; Yu, W. W.; Loh, X. J.; Li, X.; Li, P. Z. Remarkably Enhancing H_2O_2 Photogeneration by Modulating Pore‐Microenvironment of a Photoactive Covalent Organic Framework. Adv. Mater. 2025, 38, e2515517.

[8] Wu, G.; Yu, F.; Lei, H.; Xiao, S.; Song, F.; Qiu, J. Sulfone Molecular Switch Enables Direct Two‐Electron Uranium Photoreduction in Programmed Covalent Organic Frameworks. Adv. Mater. 2025, 38, e2519608.

[9] He, Y. X.; Yu, F. T.; Gui, J. L.; Zhang, Z. W.; Zhang, C. R.; Liang, R. P.; Qiu, J. D. Breaking the Exciton Bottleneck in 1D COFs via Tailored Active‐Sites Microenvironment Enables High‐Capacity Uranium Photocatalytic. Adv. Funct. Mater. 2025, 36, e2517374.

[10] Liu, C.; Wang, Y.; Dong, Z.; Zhang, Z.; Cao, X.; Zhai, Y.; Liu, Y. Covalent organic frameworks for enhanced photocatalytic extraction of uranium via the modulation of charge transfer

Just Accepted

pathways. Chem. Eng. J. 2025, 514, 163078.

[11]Hao, M.; Liu, X.; Xie, Y.; Chen, H.; Gu, H.; Luo, C.; Xiao, M.; Zhang, X.; Li, J.; Yang, X.; Zhang, J.; Yang, H.; Fan, F.; Liang, J.; Wang, X. Framework materials for nuclear waste treatment. Chem. Soc. Rev. 2026, 55, 7165-7261.

[12] Chen, Z.; Li, J.; Ma, Q.; Tai, X.; Lei, J.; Wang, X. Covalent-organic frameworks: An intelligent platform for photocatalytic uranium reduction and separation. Chin. Chem. Lett. 2026, 37, 112485.

[13]Sun, Z.; Chen, Z.; Chen, Y.; Tai, X.; Wang, S.; Lei, J.; Wang, Q.; Fan, F.; Ma, B.; Wang, X. Highly selective separation of uranium by biochar-based porous materials through sorption, precipitation, photocatalysis, and electrocatalysis strategies. Biochar. 2026, 8, 119.

[14]Choudhury, B.; Borah, B.; Choudhury, A. Extending Photocatalytic Activity of TiO2 Nanoparticles to Visible Region of Illumination by Doping of Cerium. Photochem. Photobiol. 2012, 88, 257-264.

[15]Axelsson, M.; Xia, Z.; Wang, S.; Cheng, M.; Tian, H. Role of the Benzothiadiazole Unit in Organic Polymers on Photocatalytic Hydrogen Production. JACS Au. 2024, 4, 570-577.

[16]Liang, R.; Luo, J.; Lin, S.; Li, Z.; Dong, Z.; Wu, Y.; Wang, Y.; Cao, X.; Meng, C.; Yu, F.; Liu, Y.; Zhang, Z. Boosting the photoreduction uranium activity for donor–acceptor–acceptor type conjugated microporous polymers by statistical copolymerization. Sep. Purif. Technol. 2023, 312, 123291.

[17]Zhuang, Y.; Li, W.; Yang, Q.; Li, H.; Huang, H.; Huang, X.; Long, J. Regioisomeric control of planarity enhances exciton dissociation in conjugated polymers for high-efficiency photocatalytic H_2 evolution. J. Mater. Chem. A. 2025, 13, 33318-33325.

[18]Viswanathan, V. N.; Rao, A. D.; Pandey, U. K.; Kesavan, A. V.; Ramamurthy, P. C. Molecular-level architectural design using benzothiadiazole-based polymers for photovoltaic applications. Beilstein J. Org. Chem. 2017, 13, 863-873.

[19]Wang, Y.; Michinobu, T. Benzothiadiazole and its π-extended, heteroannulated derivatives: useful acceptor building blocks for high-performance donor–acceptor polymers in organic electronics. J. Mater. Chem. C. 2016, 4, 6200-6214.

[20]Gámez-Valenzuela, S.; Comí, M.; González, S. R.; Delgado, M. C. R.; Al-Hashimi, M.; Ponce Ortiz, R. The fluorination effect: the importance of backbone planarity in achieving high performance ambipolar field effect transistors. J. Mater. Chem. C. 2023, 11, 8027-8036.

[21]An, L.; Huang, Y.; Wang, X.; Liang, Z.; Li, J.; Tong, J. Fluorination Effect for Highly Conjugated Alternating Copolymers Involving Thienylenevinylene-Thiophene-Flanked Benzodithiophene and Benzothiadiazole Subunits in Photovoltaic Application. Polymers. 2020, 12, 2073-4360.

[22]Bronstein, H.; Frost, J. M.; Hadipour, A.; Kim, Y.; Nielsen, C. B.; Ashraf, R. S.; Rand, B. P.; Watkins, S.; McCulloch, I. Effect of Fluorination on the Properties of a Donor–Acceptor Copolymer for Use in Photovoltaic Cells and Transistors. Chem. Mater. 2013, 25, 277-285.

[23]Patra, D.; Zhan, X.; Linthoinganbi, R.; Muduli, S.; Mishra, S.; Liu, Y.; Park, S. Synthesis and application of dual electron-deficient featured copolymers and their sequential fluorination for ambipolar organic thin film transistors. J. Mater. Chem. C. 2023, 11, 1457-1463.

[24] Bayarkhuu, B.; Kumar, S.; Cho, H.; Park, J.; Gashaw Seid, M.; Byun, J. Photoactive Conjugated Polyelectrolyte‐Ionomer Composite Coatings for Versatile Photoreactors. ChemCatChem. 2024, 16, e202400981.

[25]Huang, C.; Yu, W.; Fang, N.; He, C.; Chu, Y.; Lai, B. Molecular engineering of perylene diimide polymers to enhance photocatalytic performance for efficient photodegradation of ofloxacin. Sep. Purif. Technol. 2025, 360, 131146.

[26]Kumar, S.; Cho, H.; Bayarkhuu, B.; Ferguson, C. T. J.; Byun, J. From insoluble to processable: Aminic solvent dissolution of donor–acceptor conjugated network polymers for fabrication of

Just Accepted

photocatalytic thin film. Chem. Eng. J. 2024, 495, 153569.

[27] Lyons, R. J.; Sprick, R. S. Processing polymer photocatalysts for photocatalytic hydrogen evolution. Mater. Horiz. 2024, 11, 3764-3791.

[28]Moineau-Chane Ching, K. I. Impact of Alkyl-Based Side Chains in Conjugated Materials for Bulk Heterojunction Organic Photovoltaic Cells—A Review. Energies. 2023, 16, 6639.

[29]Wang, X.; Tang, A.; Chen, F.; Zhou, E. Side-chain effect in ethenylene fused thiophene-vinylene-thiophene (ETVT) based photovoltaic polymers. Polymer. 2019, 167, 31-39.

[30]Lukovskaya, E. V.; Kosmacheva, A. A.; Fedorova, O. A.; Bobyleva, A. A.; Dolganov, A. V.; Shepel', N. E.; Fedorov, Y. V.; Novikov, V. V.; Anisimov, A. V. Synthesis of chromophoric crown-containing styryl derivative of terthiophene and its complexation with octane-1,8-diaminium diperchlorate. Russ. J. Org. Chem. 2014, 50, 552-558.

[31]Pandolfi, F.; Rocco, D.; Mattiello, L. Synthesis and characterization of new D-pi-A and A-pi-D-pi-A type oligothiophene derivatives. Org. Biomol. Chem. 2019, 17, 3018-3025.

[32]Li, Z.; Lu, J.; Tse, S.-C.; Zhou, J.; Du, X.; Tao, Y.; Ding, J. Synthesis and applications of difluorobenzothiadiazole based conjugated polymers for organic photovoltaics. J. Mater. Chem. 2011, 21, 3226.

[33]Zhang, S.; Li, L.; Zhao, S.; Sun, Z.; Luo, J. Construction of Interpenetrated Ruthenium Metal–Organic Frameworks as Stable Photocatalysts for CO_2 Reduction. Inorg. Chem. 2015, 54, 8375-8379.

[34]Xu, G.; Bi, P.; Wang, S.; Xue, R.; Zhang, J.; Chen, H.; Chen, W.; Hao, X.; Li, Y.; Li, Y. Integrating Ultrathin Bulk‐Heterojunction Organic Semiconductor Intermediary for High‐Performance Low‐Bandgap Perovskite Solar Cells with Low Energy Loss. Adv. Funct. Mater. 2018, 28, 04427.

[35]Scharber, M. C.; Koppe, M.; Gao, J.; Cordella, F.; Loi, M. A.; Denk, P.; Morana, M.; Egelhaaf, H. J.; Forberich, K.; Dennler, G.; Gaudiana, R.; Waller, D.; Zhu, Z.; Shi, X.; Brabec, C. J. Influence of the Bridging Atom on the Performance of a Low‐Bandgap Bulk Heterojunction Solar Cell. Adv. Mater. 2010, 22, 367-370.

[36]Zhao, Z.; Zheng, Y.; Wang, C.; Zhang, S.; Song, J.; Li, Y.; Ma, S.; Cheng, P.; Zhang, Z.; Chen, Y. Fabrication of Robust Covalent Organic Frameworks for Enhanced Visible-Light-Driven H2 Evolution. ACS Catal. 2021, 11, 2098-2107.

[37]Zhou, F.; Dong, Z.; Dong, Y.; Chen, J.; Wang, Y.; Wang, Y.; Lin, Z.; Zhang, Z.; Liu, Y.; Han, B. Regulation of piezoelectric polarization for uranium extraction dynamics by spatially gradient manipulation of oxygen vacancies. Appl. Catal. B Environ. Energy. 2026, 390, 126603.

[38]Zhang, S.; Du, M.; Xing, Z.; Li, Z.; Pan, K.; Zhou, W. Defect-rich and electron-rich mesoporous Ti-MOFs based NH_2-MIL-125(Ti)@$ZnIn_2S_4$/CdS hierarchical tandem heterojunctions with improved charge separation and enhanced solar-driven photocatalytic performance. App. Catal. B: Environ. 2020, 262, 118202.

[39] Yu, B.; Zhang, L.; Wu, H.; Wen, J.; Mahmood Ali, A.; Zhang, H.; Zhang, G.; Yu, M. Plasma-Treated F modified TiO2 impact to enhance the photocatalytic performance of TiO_2. Chem. Phys. Lett. 2022, 801, 139710.

[40]Huang, Z. W.; Li, X. B.; Mei, L.; Han, Y. Z.; Song, Y. T.; Fu, X.; Zhang, Z. H.; Guo, Z. J.; Zeng, J. R.; Bian, F. G.; Wu, W. S.; Hu, K. Q.; Shi, W. Q. All‐in‐One: Photo‐Responsive Lanthanide‐Organic Framework for Simultaneous Sensing, Adsorption, and Photocatalytic Reduction of Uranium. Adv. Funct. Mater. 2024, 34, 4126.

[41]Ma, Z.; Sun, C.; Lin, D.; Yao, W.; Hou, H.; Wu, D.; Guo, X.; Yu, X.; Wang, X. Exploiting the nodes of metal-organic framework by grafting functional organic molecules for synergistic uranium extraction. Sep. Purif. Technol. 2025, 359,

Just Accepted

130607.

[42]Liu, J.-L.; Lin, M.-X.; Huang, J.; Zhang, C.-R.; Qi, J.-X.; Cai, Y.-J.; Chen, X.-J.; Zhang, L.; Liang, R.-P.; Qiu, J.-D. sp^2-c linked Cu-based metal-covalent organic framework for chemical and photocatalysis synergistic reduction of uranium. Chem. Eng. J. 2024, 491, 151982.

[43]Li, M.; Zhou, F.; Dai, Z.; Wei, S.; Wang, J.; Wang, Y.; Cao, Y.; Wang, H.; Li, J.; Huang, J.; Liu, Y. N. Integration of heterojunction and pore wall engineering on functionalized covalent organic frameworks for boosting photocatalytic reduction of uranium. J. Colloid Interface Sci. 2025, 699, 138180.

[44]Wang, X.-X.; Zhang, R.; Peng, Z.-H.; Gong, J.-W.; Hu, E.-M.; Niu, C.-P.; Liang, R.-P.; Qiu, J.-D. Nickel complex-bridging to enhance electron transport in covalent organic frameworks for efficient photocatalytic uranium reduction. Chem. Eng. J. 2025, 521, 167061.

[45]Yu, F.; Zhu, Z.; Li, C.; Li, W.; Liang, R.; Yu, S.; Xu, Z.; Song, F.; Ren, Q.; Zhang, Z. A redox-active perylene-anthraquinone donor-acceptor conjugated microporous polymer with an unusual electron delocalization channel for photocatalytic reduction of uranium (VI) in strongly acidic solution. App. Catal. B: Environ. 2022, 314, 121467.

[46]Huang, H.; Yang, L.; Facchetti, A.; Marks, T. J. Organic and Polymeric Semiconductors Enhanced by Noncovalent Conformational Locks. Chem. Rev. 2017, 117, 10291-10318.

[47]Wang, M.; Fu, S.; Petkov, P.; Fu, Y.; Zhang, Z.; Liu, Y.; Ma, J.; Chen, G.; Gali, S. M.; Gao, L.; Lu, Y.; Paasch, S.; Zhong, H.; Steinrück, H.-P.; Cánovas, E.; Brunner, E.; Beljonne, D.; Bonn, M.; Wang, H. I.; Dong, R.; Feng, X. Exceptionally high charge mobility in phthalocyanine-based poly(benzimidazobenzophenanthroline)-ladder-type two-dimensional conjugated polymers. Nat. Mater. 2023, 22, 880-887.

[48]Sun, S.-J.; Menšík, M.; Toman, P.; Gagliardi, A.; Král, K. Influence of acceptor on charge mobility in stacked π-conjugated polymers. Chem. Phys. 2018, 501, 8-14.

[49]Zhang, G.; Yang, J.; Lan, Z.; Shan, C.; Lin, Q.; Ke, Y.; Cai, Y.; Chen, H.; Jin, Z.; Zhang, X.; Peng, Q.; Huang, H. Tuning the physicochemical properties of conjugated polymers via intramolecular noncovalent interactions. Sci. China Mater.2025, 68, 4173-4181.

[50]Yu, F.; Yu, S.; Li, C.; Li, Z.; Song, F.; Xu, Z.; Zhu, Y.; Dai, C.; Cao, X.; Zhang, Z.; Liu, Y.; Qiu, J. Molecular engineering of biomimetic donor-acceptor conjugated microporous polymers with full-spectrum response and an unusual electronic shuttle for enhanced uranium(VI) photoreduction. Chem. Eng. J. 2023, 466, 143285.

[51]Deng, Z.; Zhao, H.; Cao, X.; Xiong, S.; Li, G.; Deng, J.; Yang, H.; Zhang, W.; Liu, Q. Enhancing Built-in Electric Field via Molecular Dipole Control in Conjugated Microporous Polymers for Boosting Charge Separation. ACS Appl. Mater. Interfaces. 2022, 14, 35745-35754.

[52]Yu, F.; Li, C.; Li, W.; Yu, Z.; Xu, Z.; Liu, Y.; Wang, B.; Na, B.; Qiu, J. Π‐Skeleton Tailoring of Olefin‐Linked Covalent Organic Frameworks Achieving Low Exciton Binding Energy for Photo‐Enhanced Uranium Extraction from Seawater. Adv. Funct. Mater. 2023, 34, 2307230.

[53]Wang, H.; Mei, P.; Huang, X.; Xiao, J.; Sun, Y. Uranyl(VI) boosting 3D g-C_3N_4 photocatalytic H_2O_2 production for U(VI) immobilization. J. Cleaner Prod. 2022, 330, 129821.

Just Accepted

Electronic Supplementary Material

Solution-processable conjugated polymer films via fluorination-induced noncovalent conformational locks for efficient photocatalytic U(VI) removal

Zuojia Li[1,2], Jinwei Shi[1,2], Hanting Wu[2], Yuanping Jiang[1,2] ✉, Zhibin Zhang[1,2] ✉, Yunhai Liu[2,3]

[1]*Jiangxi Province Key Laboratory of Nuclear Physics and Technology, East China University of Technology, Nanchang 330013, China*
[2]*School of Chemistry and Materials Science, East China University of Technology, Nanchang 330013, China*
[3]*Gandong University, Fuzhou 344000, China*

✉ Address correspondence to Zhibin Zhang, zhbzhang@ecut.edu.cn; Yuanping Jiang, jypjiang@ecut.edu.cn

Supporting information to https://doi.org/10.26599/NR.2026.94909283

1. Experimental Section..... 19
1.1 Photocatalytic Removal of Uranium..... 19
1.2 Cycle elution experiment..... 19
1.3 Electrochemical measurement..... 19
1.4 DFT calculation methods..... 19
2. Characterization..... 21
3. Nuclear Magnetic Resonance..... 28
4. References:..... 32

Just Accepted

1. Experimental Section

1.1 Photocatalytic Removal of Uranium

A uranyl nitrate stock solution (50 ppm) was prepared by dissolving an appropriate amount of $UO_2(NO_3)_2 \cdot 6H_2O$ in nitric acid solution in a jacketed quartz beaker reactor, which was cooled by circulating water. The pH of the solution was adjusted using aqueous HNO_3 or Na_2CO_3. Subsequently, 10 mg of the material was added to 50 mL of UO_2^{2+} solution (50 ppm). Prior to irradiation, the mixture was continuously stirred in the dark for 1 h to achieve adsorption-desorption equilibrium. Then, 2 mL of methanol solution was added, and the solution was irradiated for 4 h using a 300-W-CEL-HXF300-T3-Xe lamp equipped with a 400 nm cutoff filter. At specific intervals, 2.0 mL aliquots were precisely withdrawn, filtered through a 0.22 μm nylon syringe filter to remove solid particles, and the resulting clear supernatant was analyzed for uranium(VI) concentration via UV-Vis spectrophotometry. Specifically, Arsenazo III was used as the chromogenic reagent, and absorbance was measured at a wavelength of 650 nm.

1.2 Cycle elution experiment

After the photocatalysis is completed, filter the photocatalytic material, wash the material with a 0.2 mol/L Na_2CO_3 solution under stirring for 6 h. After that, wash it with ethanol and deionized water and dry it for the next experiment.

1.3 Electrochemical measurement

Electrochemical measurements including Mott-Schottky (M-S) plots, electrochemical impedance spectroscopy (EIS), and transient photocurrent responses (I-t) were performed on a DH7000 electrochemical workstation using a three-electrode system. A 0.5 M aqueous Na_2SO_4 solution served as the electrolyte, and a 300 W xenon lamp equipped with a 420 nm cutoff filter was used as the light source. A platinum auxiliary electrode and a saturated Ag/AgCl electrode were employed as the counter electrode and reference electrode, respectively, while a glassy carbon electrode loaded with the as-prepared material served as the working electrode.

For the transient photocurrent (i-t) measurements, the working electrode was prepared as follows: 5.0 mg of the synthesized material was ground with 0.05 mL of 5% Nafion aqueous solution and 0.5 mL of ethanol to form a homogeneous slurry. The resulting slurry was then cast onto an ITO glass electrode with an active area of 2.5 cm^2, followed by drying at 60 ºC for 1 h to evaporate the solvent. The photocurrent intensity of the prepared electrode was measured by repeatedly turning the light source on and off.

1.4 DFT calculation methods

To investigate the electrostatic potential and molecular orbitals of the materials, density functional theory (DFT) calculations were performed using Gaussian16. The 6-311G(d) basis set and associated pseudopotentials were employed for all H, C, N, S, and F atoms. The ECP60MWB basis set was used for all U atoms. Energy calculations were performed without additional corrections and employed tight convergence criteria. The adsorption energy was calculated according to the following equation:

$$E_{ads} = E_{total} - (E_{slab} + E_U)$$

where Eads is the adsorption energy (kcal/mol) of UO_2^{2+} on the substrate material, Etotal is the total energy of the adsorbed system (kcal/mol), Eslab is the energy of the substrate material (kcal/mol), and EU is the energy of UO_2^{2+} (kcal/mol). Geometry optimizations and frequency calculations were performed in aqueous solution using the SMD solvation model. Hole-electron and electrostatic potential analyses were carried out using the Multiwfn software package, and the visualized energy levels and electrostatic potential distributions were plotted with the aid of VMD[1].

Just Accepted

2.Characterization

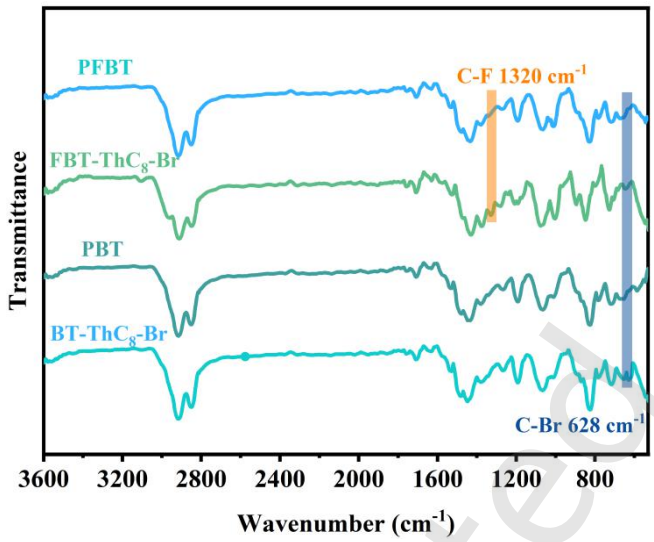


Fig. S1 The Fourier transform infrared (FTIR) spectra of PFBT, FBT-ThC$_8$-Br, PBT, and BT-ThC$_8$-Br.

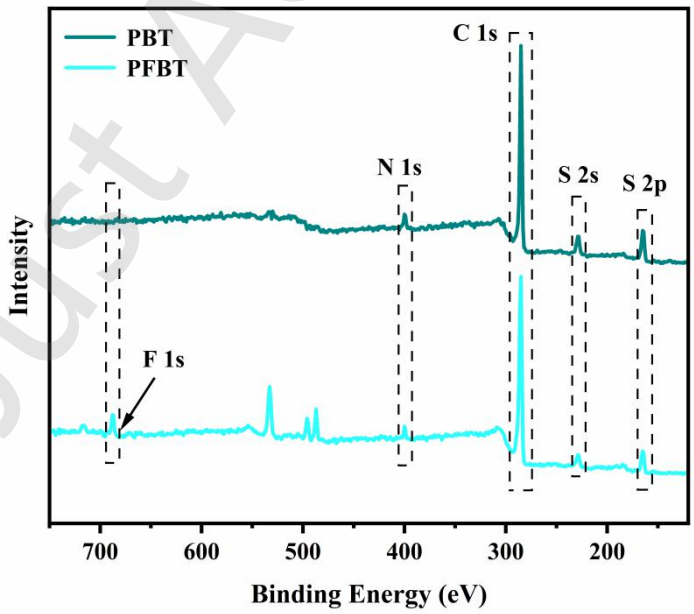


Fig. S2 XPS survey spectra of PBT and PFBT polymers

Just Accepted

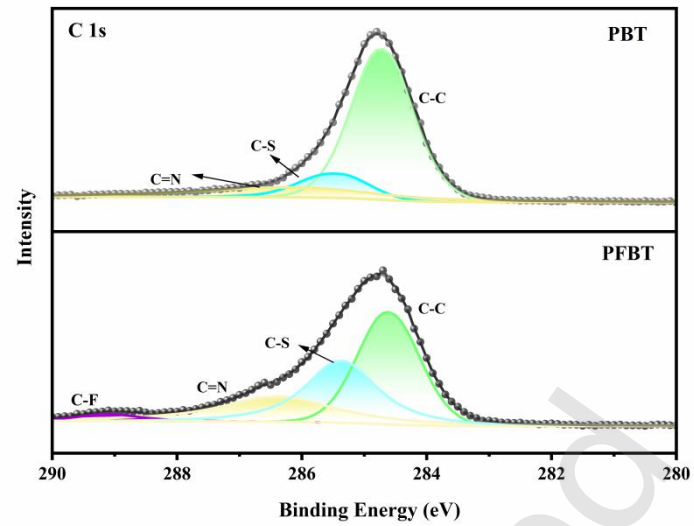


Fig. S3 High-resolution C 1s spectra

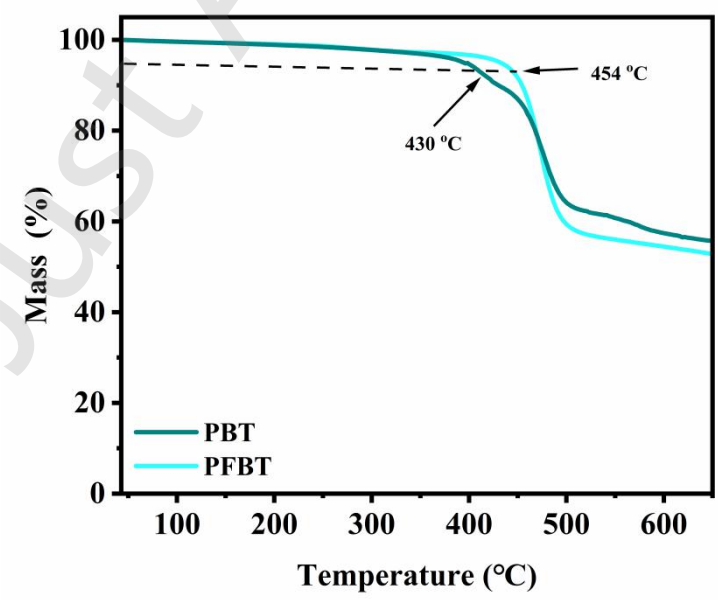


Fig. S4 Thermogravimetric analysis (TGA) curves of PBT and PFBT.

Just Accepted

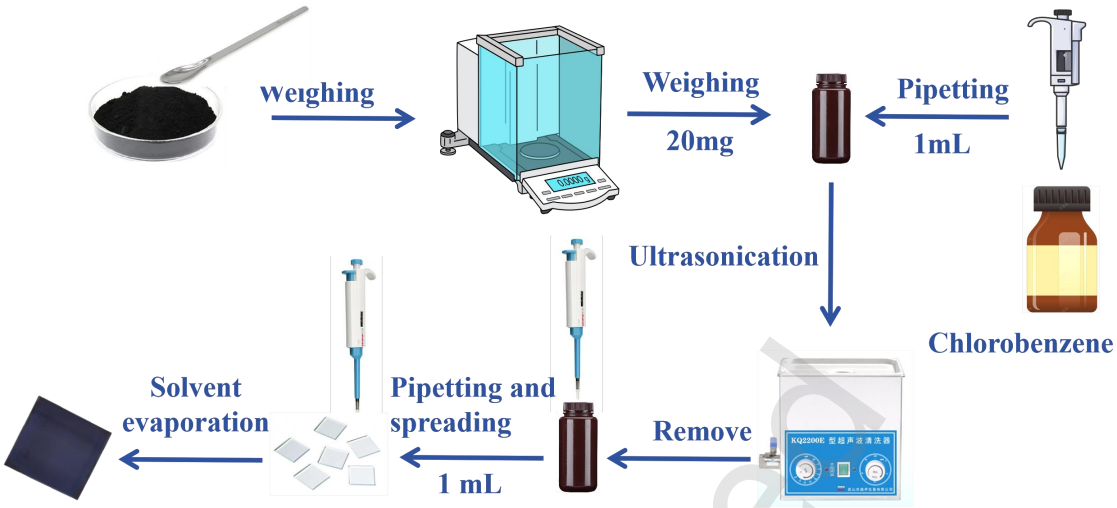


Fig. S5 The preparation process of Film-PBT and Film-PFBT.

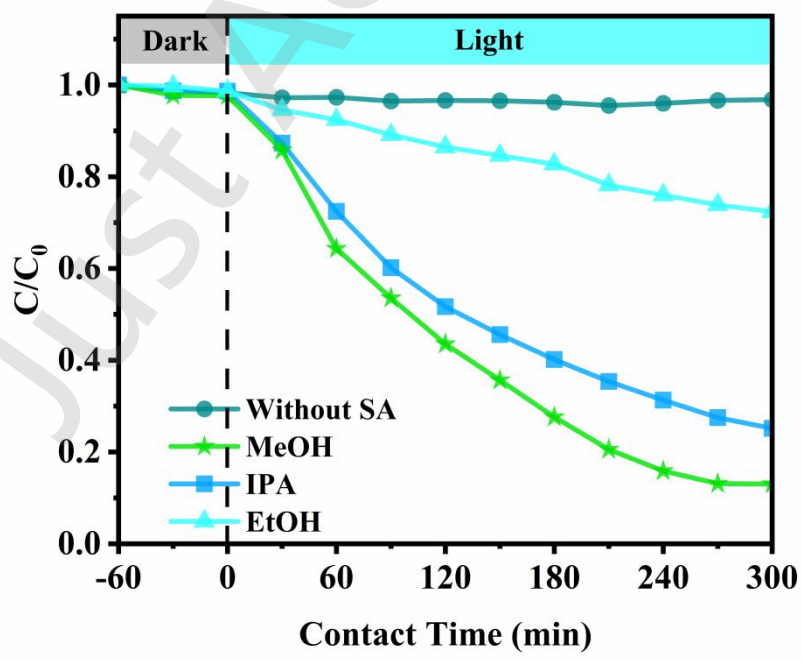


Fig. S6 Photocatalytic U(VI) removal performance curves of Film-PBT using different sacrificial agents.

Just Accepted

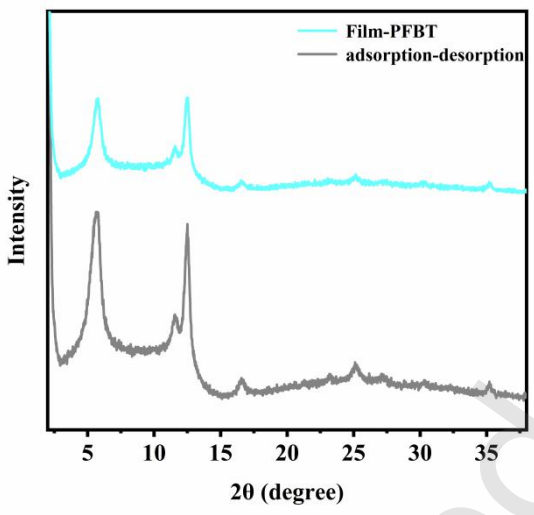


Fig. S7 XRD patterns of the pristine Film-PFBT and the Film-PFBT after adsorption-desorption cycles.

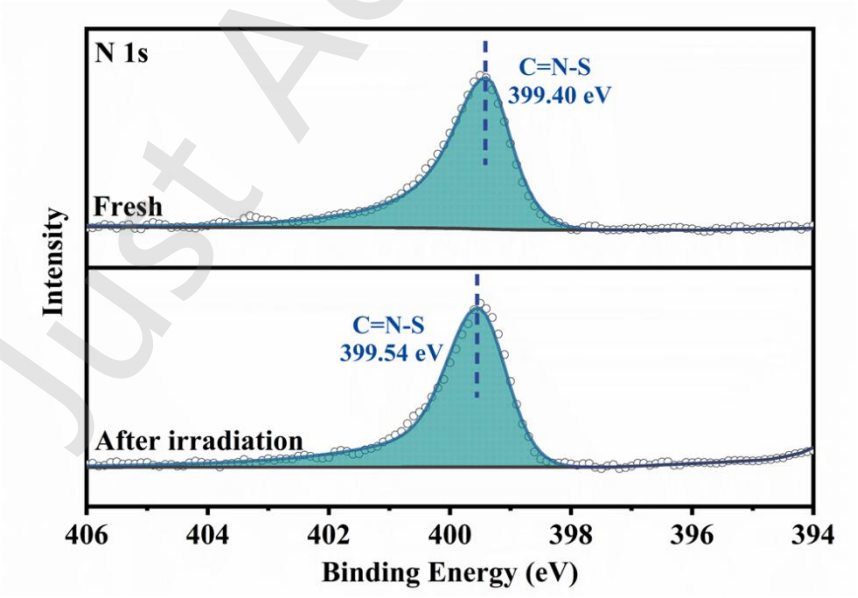


Fig. S8 High-resolution N 1s XPS spectra of Film-PFBT after photocatalysis.

Just Accepted

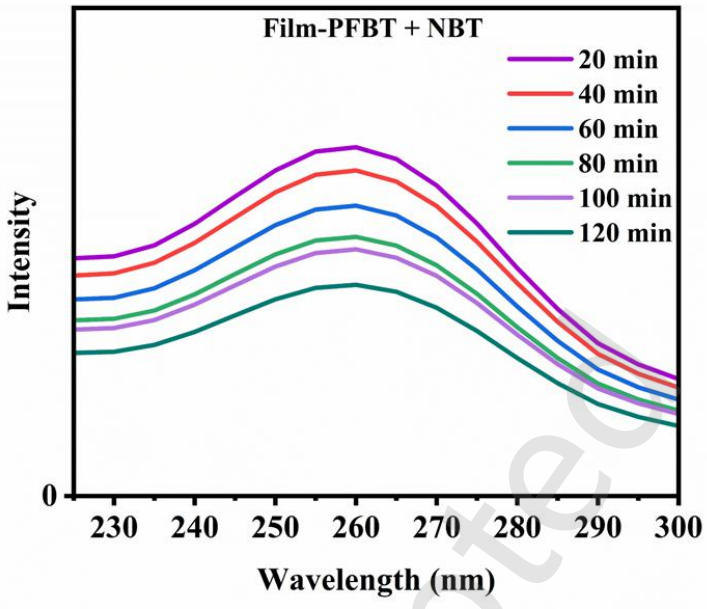


Fig. S9 Fluorescence curve of NBT under light irradiation.

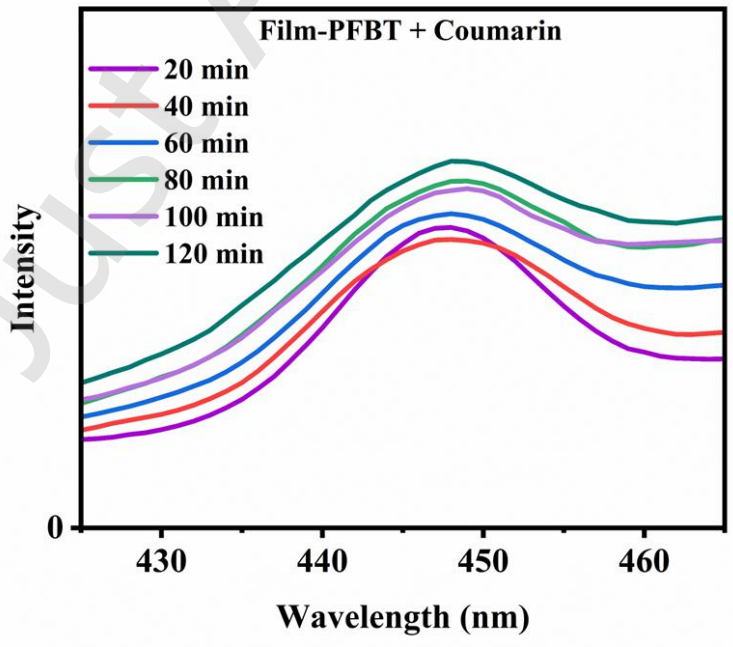


Fig. S10 Fluorescence curve of coumarin under light irradiation.

Just Accepted

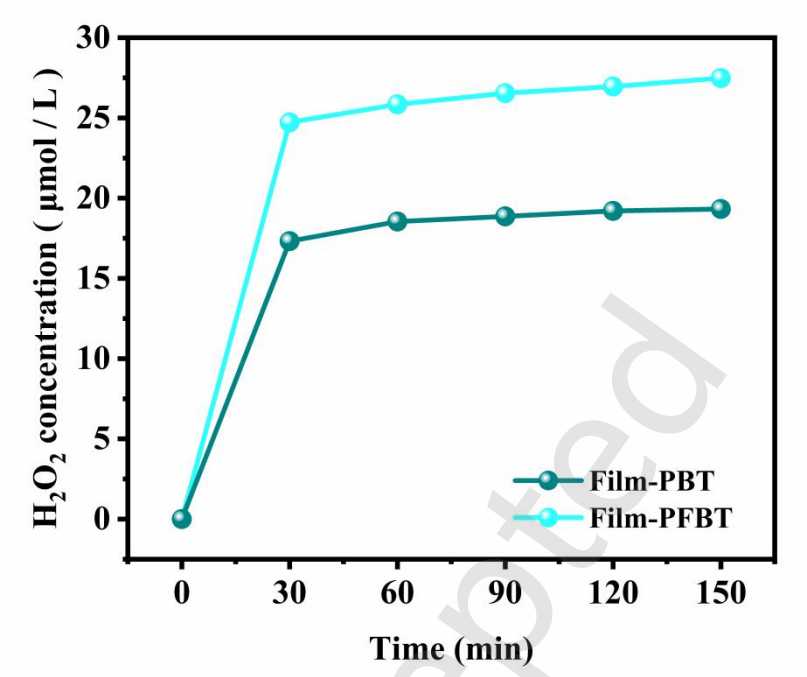


Fig. S11 Concentration variation curves of H_2O_2 generated by Film-PFBT and Film-PBT under light irradiation.

Just Accepted

Table S1 Comparison of uranium removal performance of different materials under their respective optimal pH conditions

Materials	Conditions	Maximum removal rate(%)	Citation
IHEP-24	50ppmU(Ⅵ), pH=5.5	80.4	2
MOF-808@OxA	50ppmU(Ⅵ)，pH=6	80.6	3
Cu-TMT	50ppmU(Ⅵ)，pH=5	93.4	4
NH_2-MX@Por-COF-OMe	50ppmU(Ⅵ)，pH=6	92.8	5
$Ni(bipy)_3$@COF	50ppmU(Ⅵ)，pH=5	84.5	6
ECUT-AQ	50ppmU(Ⅵ)，pH=4	73.4	7

Table S2 Comparison of the key dihedral angles (θ_1, θ_2, θ_3) and conformation-lock types of the PBT and PFBT molecular backbones obtained from DFT calculation

Conjugated polymer	Type of conformational lock	Dihedral angle θ_1	Dihedral angle θ_2	Dihedral angle θ_3
PBT	No conformational lock	0.32°	6.08°	44.34°
PFBT	Semi-conformational lock	0.21°	0.91°	30.99°

Just Accepted

3.Nuclear Magnetic Resonance

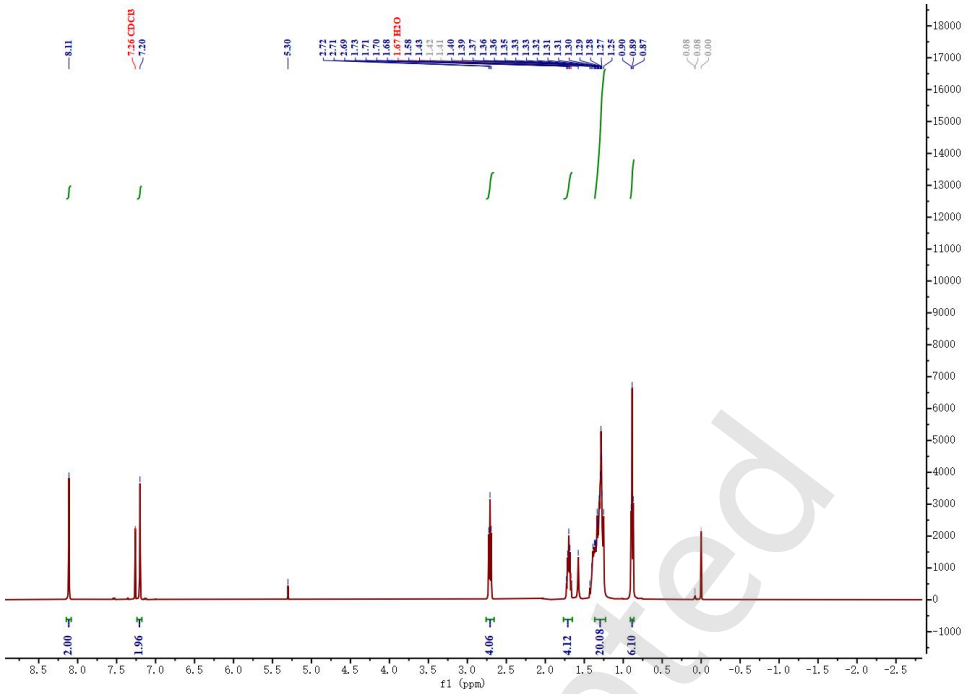


Fig. S12 The ^{1}H NMR (500 MHz) of 5, 6-difluoro-4, 7-bis(4-octyl-2-thienyl)-benzothiadiazole in $CDCl_3$

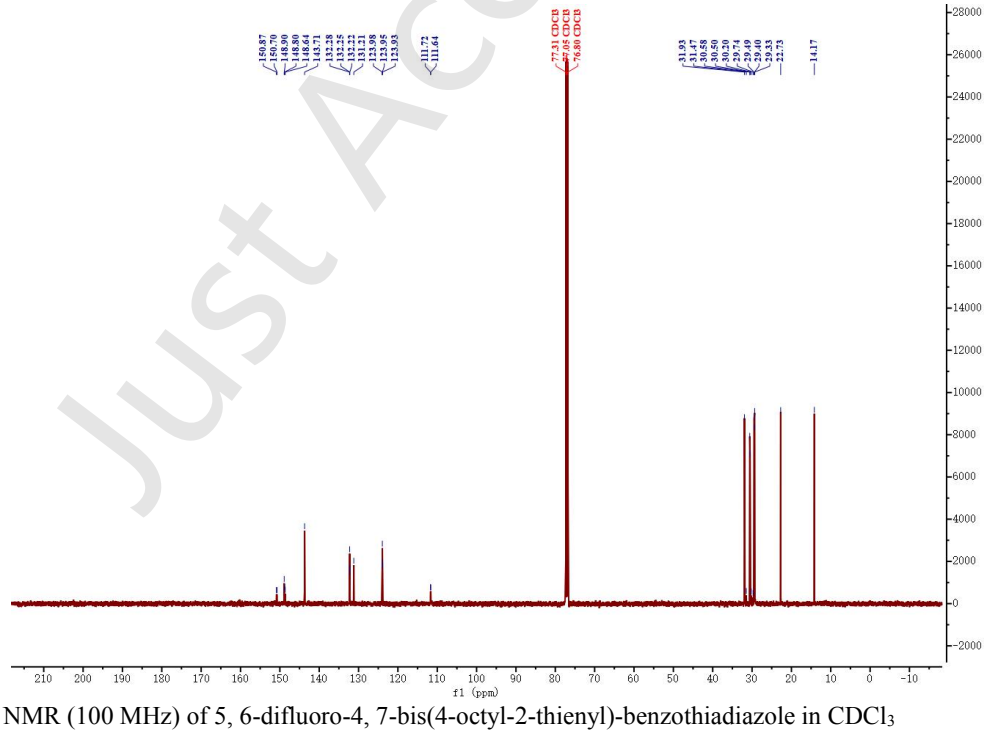


Fig. S13 The ^{13}C NMR (100 MHz) of 5, 6-difluoro-4, 7-bis(4-octyl-2-thienyl)-benzothiadiazole in $CDCl_3$

Just Accepted

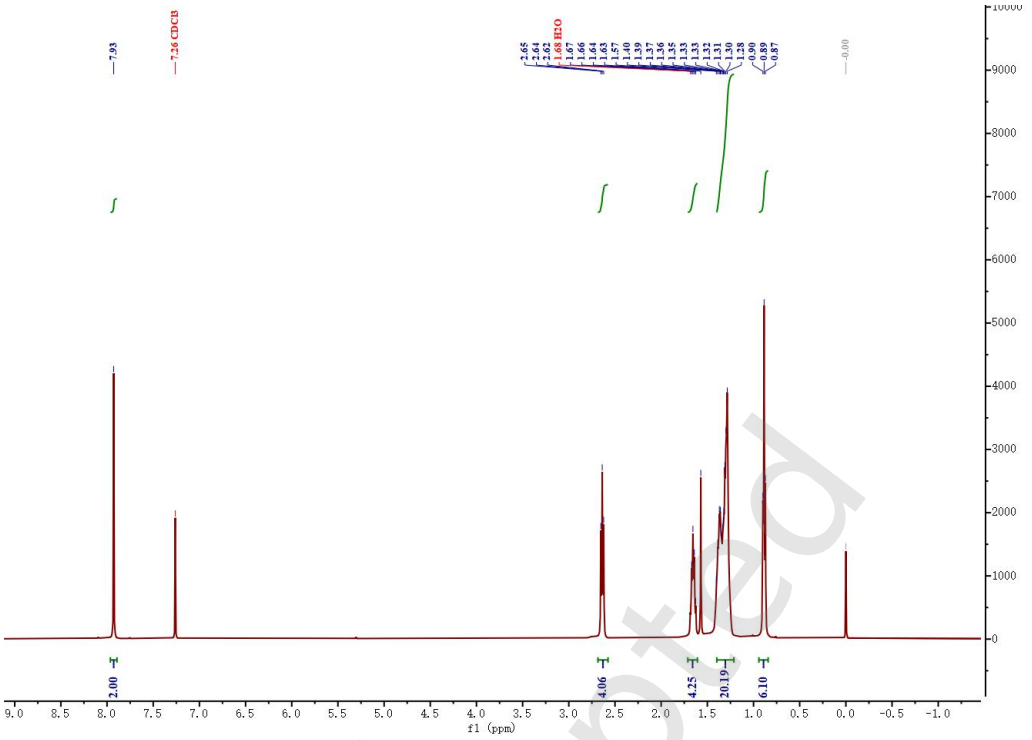


Fig. S14 The ^{1}H NMR (500 MHz) of FBT-ThC_8-Br in $CDCl_3$

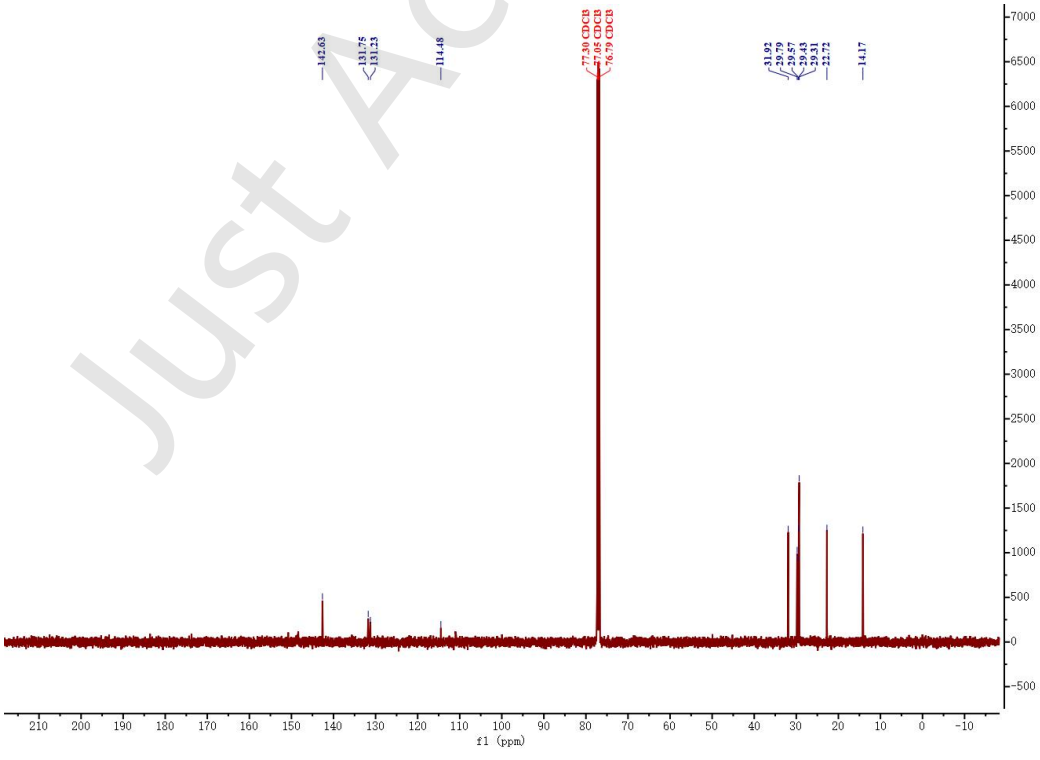


Fig. S15 The ^{13}C NMR (100 MHz) of FBT-ThC_8-Br in $CDCl_3$

Just Accepted

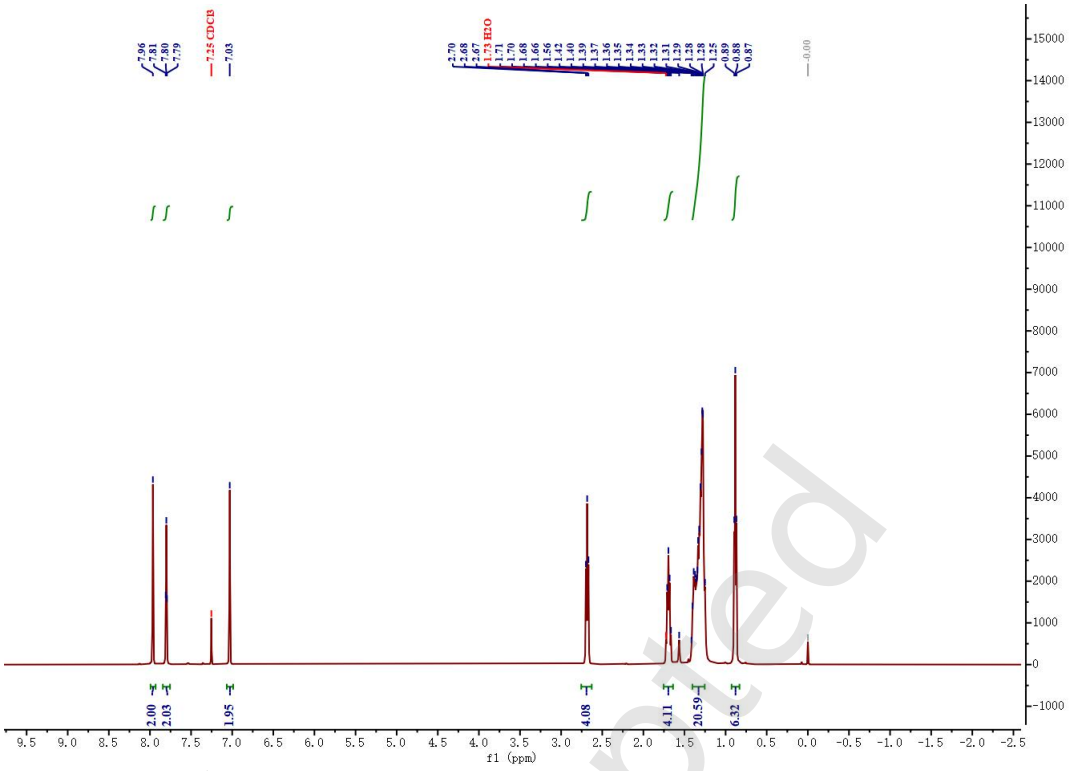


Fig. S16 ^{1}H NMR (500 MHz) of 4, 7-bis(4-octyl-2-thienyl)-benzothiadiazole in $CDCl_3$

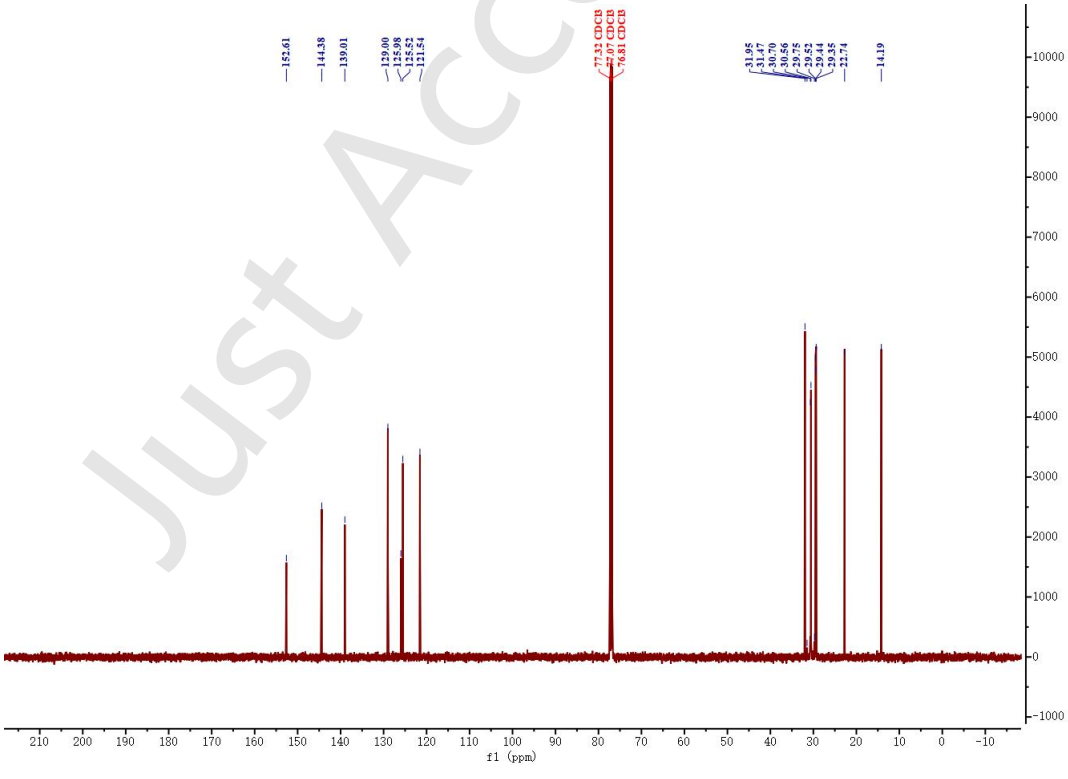


Fig. S17 ^{13}C NMR (100 MHz) of 4, 7-bis(4-octyl-2-thienyl)-benzothiadiazole in $CDCl_3$

Just Accepted

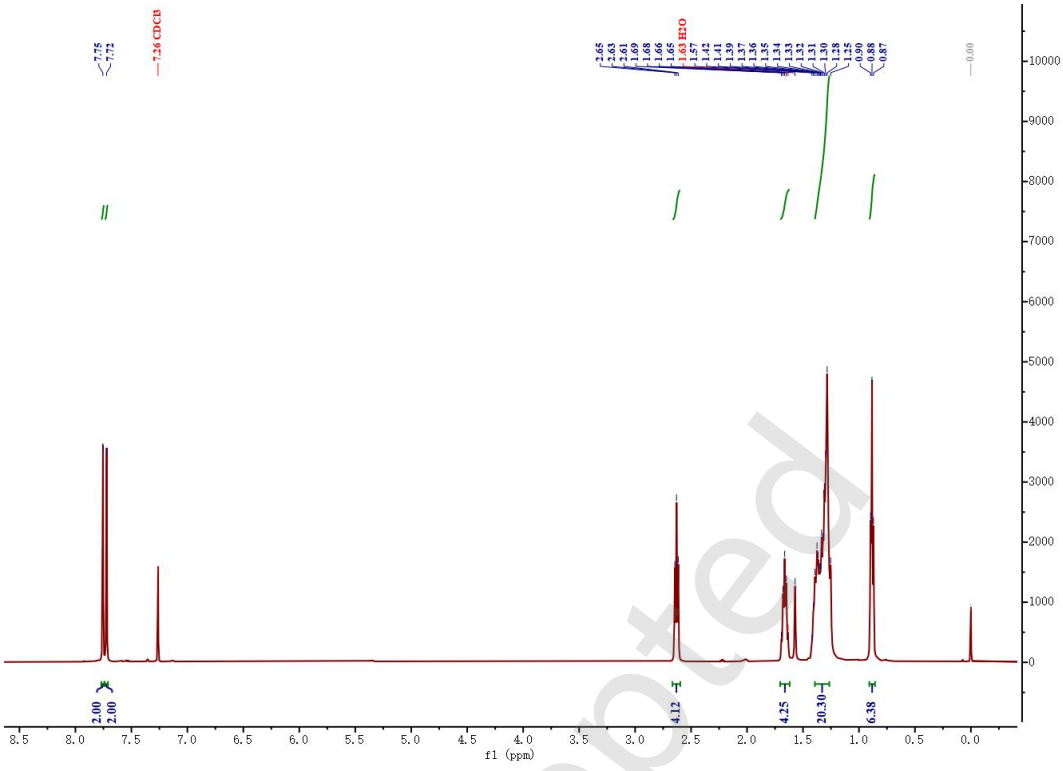


Fig. S18 ^{1}H NMR (500 MHz) of BT-ThC$_8$-Br in CDCl$_3$

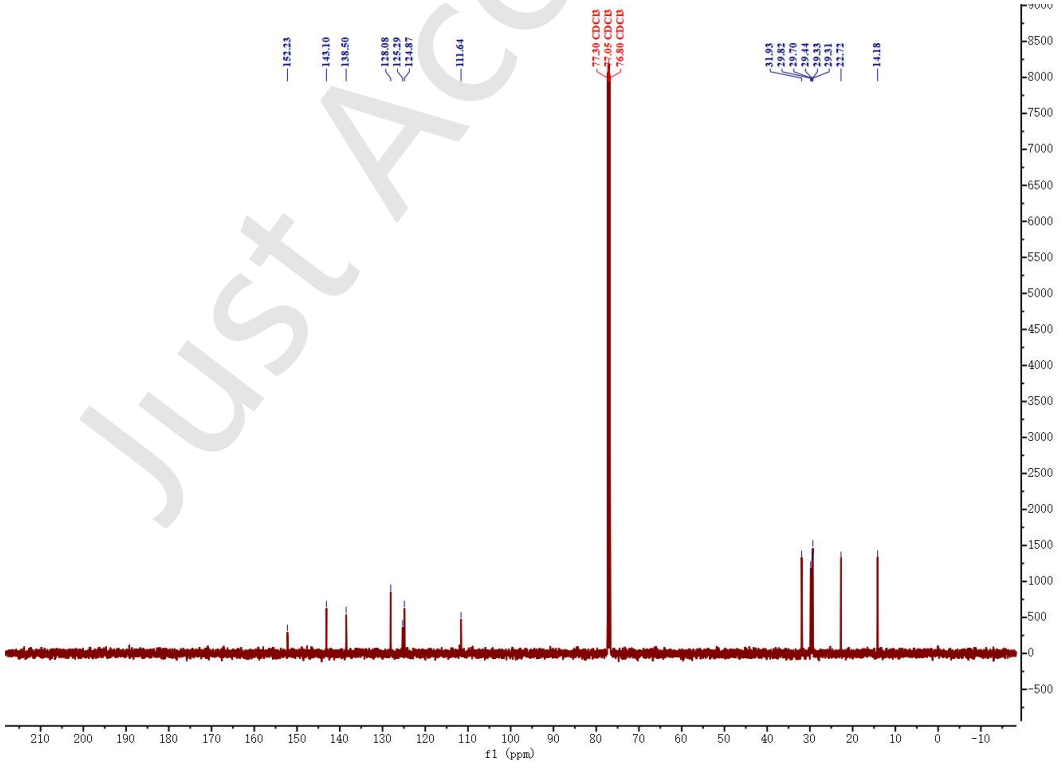


Fig. S19 ^{13}C NMR (100 MHz) of BT-ThC$_8$-Br in CDCl$_3$

Just Accepted

3.References:

[1]Lu, T.; Chen, F. Multiwfn: A multifunctional wavefunction analyzer. J. Comput. Chem. 2011, 33, 580-592.

[2]Huang, Z. W.; Li, X. B.; Mei, L.; Han, Y. Z.; Song, Y. T.; Fu, X.; Zhang, Z. H.; Guo, Z. J.; Zeng, J. R.; Bian, F. G.; Wu, W. S.; Hu, K. Q.; Shi, W. Q. All‐in‐One: Photo‐Responsive Lanthanide‐Organic Framework for Simultaneous Sensing, Adsorption, and Photocatalytic Reduction of Uranium. Adv. Funct. Mater. 2024, 34, 4126.

[3]Ma, Z.; Sun, C.; Lin, D.; Yao, W.; Hou, H.; Wu, D.; Guo, X.; Yu, X.; Wang, X. Exploiting the nodes of metal-organic framework by grafting functional organic molecules for synergistic uranium extraction. Sep. Purif. Technol. 2025, 359, 130607.

[4]Liu, J.-L.; Lin, M.-X.; Huang, J.; Zhang, C.-R.; Qi, J.-X.; Cai, Y.-J.; Chen, X.-J.; Zhang, L.; Liang, R.-P.; Qiu, J.-D. sp2-c linked Cu-based metal-covalent organic framework for chemical and photocatalysis synergistic reduction of uranium. Chem. Eng. J. 2024, 491, 151982.

[5]Li, M.; Zhou, F.; Dai, Z.; Wei, S.; Wang, J.; Wang, Y.; Cao, Y.; Wang, H.; Li, J.; Huang, J.; Liu, Y. N. Integration of heterojunction and pore wall engineering on functionalized covalent organic frameworks for boosting photocatalytic reduction of uranium. J. Colloid Interface Sci. 2025, 699, 138180.

[6]Wang, X.-X.; Zhang, R.; Peng, Z.-H.; Gong, J.-W.; Hu, E.-M.; Niu, C.-P.; Liang, R.-P.; Qiu, J.-D. Nickel complex-bridging to enhance electron transport in covalent organic frameworks for efficient photocatalytic uranium reduction. Chem. Eng. J. 2025, 521, 167061.

[7]Yu, F.; Zhu, Z.; Li, C.; Li, W.; Liang, R.; Yu, S.; Xu, Z.; Song, F.; Ren, Q.; Zhang, Z. A redox-active perylene-anthraquinone donor-acceptor conjugated microporous polymer with an unusual electron delocalization channel for photocatalytic reduction of uranium (VI) in strongly acidic solution. App. Catal. B: Environ. 2022, 314, 121467.

Just Accepted